NASA TECHNICAL MEMORANDUM

NASA TM X-2302

NASA TM X-2302

METHOD FOR PREDICTING COMPRESSIBLE TURBULENT BOUNDARY LAYERS IN ADVERSE PRESSURE GRADIENTS

by S. Z. Pinckney

Langley Research Center
Hampton, Va. 23365

NATIONAL AERONAUTICS AND SPACE ADMINISTRATION • WASHINGTON, D. C. • AUGUST 1971

1. Report No.	2. Government Accession No.	3. Recipient's Catalog No.
NASA TM X-2302		

4. Title and Subtitle	5. Report Date
METHOD FOR PREDICTING COMPRESSIBLE TURBULENT BOUNDARY LAYERS IN ADVERSE PRESSURE GRADIENTS	August 1971
	6. Performing Organization Code
7. Author(s)	8. Performing Organization Report No.
S. Z. Pinckney	L-6802
	10. Work Unit No.
9. Performing Organization Name and Address	764-75-01-01
NASA Langley Research Center Hampton, Va. 23365	11. Contract or Grant No.
	13. Type of Report and Period Covered
12. Sponsoring Agency Name and Address	Technical Memorandum
National Aeronautics and Space Administration Washington, D.C. 20546	14. Sponsoring Agency Code

15. Supplementary Notes

16. Abstract

In connection with research programs on hypersonic airbreathing propulsion, an integral method for predicting boundary-layer development in transition and turbulent-flow regions on two-dimensional or axisymmetric bodies has been developed through use of the integral-momentum, moment-of-momentum, and energy equations together with appropriate auxiliary equations. The method has the capability of predicting nonequilibrium velocity distributions. It employs some simplifying assumptions, such as flat-plate friction and heat-transfer coefficients, no provision for a normal-pressure gradient, and perfect-gas relations; therefore, the method is considered interim in nature.

Extensive comparisons have been made with data covering a wide Mach number range, cooled and uncooled walls, two-dimensional and axisymmetric bodies with and without regions of longitudinal-pressure gradient, and a few cases with strong normal-pressure gradients. The overall conclusion is that the method will predict the displacement, momentum, and boundary-layer thickness of the data within the limits of the experimental accuracy.

17. Key Words (Suggested by Author(s))	18. Distribution Statement
Boundary layer Turbulent boundary layer Transitional boundary layer	Unclassified – Unlimited

19. Security Classif. (of this report)	20. Security Classif. (of this page)	21. No. of Pages	22. Price*
Unclassified	Unclassified	58	$3.00

*For sale by the National Technical Information Service, Springfield, Virginia 22151

METHOD FOR PREDICTING COMPRESSIBLE TURBULENT BOUNDARY LAYERS IN ADVERSE PRESSURE GRADIENTS

By S. Z. Pinckney
Langley Research Center

SUMMARY

In connection with research programs on hypersonic airbreathing propulsion, an integral method for predicting boundary-layer development in transition and turbulent-flow regions on two-dimensional or axisymmetric bodies has been developed through use of the integral-momentum, moment-of-momentum, and energy equations together with appropriate auxiliary equations. The method has the capability of predicting nonequilibrium velocity distributions. It employs some simplifying assumptions, such as flat-plate friction and heat-transfer coefficients, no provision for a normal-pressure gradient, and perfect-gas relations; therefore, the method is considered interim in nature.

Extensive comparisons have been made with data covering a wide Mach number range, cooled and uncooled walls, two-dimensional and axisymmetric bodies with and without regions of longitudinal-pressure gradient, and a few cases with strong normal-pressure gradients. The overall conclusion is that the method will predict the displacement, momentum, and boundary-layer thickness of the data within the limits of the experimental accuracy.

INTRODUCTION

Interest in hypersonic vehicles employing airbreathing propulsion has increased in recent years as a result of several studies describing a number of promising applications. A general summary and the evaluation of these studies are given in reference 1, and one of the applications, the reusable airbreathing booster, is discussed in some detail in references 2 and 3. Before any of these vehicles can become operational, however, several technology advances have to be achieved, particularly in the area of integrated engine concept development. A critical part of this work is the design and performance prediction of hypersonic inlets, which require adequate methods for predicting boundary-layer growth on the surfaces. In particular these boundary layers are developed in the presence of positive and negative pressure gradients.

In selecting or generating a design tool the engineer sometimes must make a compromise choice between the high potential accuracy and detail of one method and the simplicity and convenience of a less accurate and less complex one. This situation particularly pertains to boundary-layer-prediction methods which are applicable to flows in pressure gradients and for which the choices cover a very large range; pertinent comments by a select panel of specialists on the subject are contained in reference 4, where, for instance, advocates of both finite difference and integral techniques present arguments. Similarly, in reference 5 the relative merits of various finite-difference and integral techniques are discussed. Finite-difference methods inherently can produce much detailed information on the boundary layer, and much progress has been made in recent years in formulating these methods (for example, refs. 6 to 9). It is also evident that detailed information can be generated with integral methods (for example, refs. 10 to 12). Since the technology for transitional and turbulent boundary layers still is being developed and major features are still empirical, the type of method selected to perform a given job depends on the nature of the calculation required. The detailed assumptions that are made in any particular method are the important considerations. In this regard a general review is made of some of the integral methods that have been used in hypersonic inlet work, and problem areas encountered are noted.

The first step in a prediction method is to compute the laminar boundary-layer development up to the point where transition is initiated; this point generally is selected by using available data as a guide or using an empirical criterion. Several laminar methods such as reference 13 are available. In the transition region the simplest procedure is to assume that the entire transition from laminar to turbulent flow occurs in the plane where transition is initiated while one integral parameter, such as the displacement thickness (ref. 13), remains constant. Another approach would be to allow transition to extend over a finite length of surface (ref. 14). In the turbulent region a relatively simple procedure is to perform a simultaneous solution of the integral-momentum and energy equations with assumptions of flat-plate friction and heat transfer, equilibrium flat-plate velocity profiles, and the Crocco temperature-velocity profile (refs. 13 to 15). In a pressure gradient the methods of references 13 to 15 are unable to predict accurately either the boundary-layer velocity profiles or total mass in the boundary layer. In contrast to the methods of references 13 to 15, another approach to the problem consists of the simultaneous solution of the momentum and moment-of-momentum equations as presented in reference 16. In order to express the moment-of-momentum equation in terms of the form factor, power-law velocity profiles were used, a functional relation between the shear stress integral and the form factor was assumed, and integrals of the enthalpy profiles were assumed to have the same functional relation to the form factor as in laminar flows. With the inclusion of the moment-of-momentum equation, the method of reference 16 did include provisions for nonequilibrium velocity profiles. In reference 16

the ability to predict nonequilibrium velocity profiles and the inclusion of the shear stress integral as a function of the form factor results in better velocity profile and boundary-layer mass-flow predictions. However, with surface heat transfer the simultaneous solution must be accomplished with the inclusion of the energy equation. In the study of reference 17 it was concluded that provisions for nonequilibrium velocity profiles were needed to obtain accurate predictions of the data; also, previous work (ref. 18) has indicated that a modification of the Crocco-type relation for the temperature profile provides higher accuracy.

The purpose of the present paper is to present an integral method for boundary-layer prediction through the transition and turbulent regions of two-dimensional or axisymmetric bodies. The method was developed during the course of a hypersonic-inlet research program with particular emphasis on applicability to the computation of boundary layers in the presence of inlet-type pressure gradients. Some preliminary results from the inlet experiments and comparisons with predictions using an early version of the boundary-layer method are given in reference 17, which discusses deficiencies of the initial method as determined by comparisons with the data. With these deficiencies in mind the initial version was modified so as to overcome these problems. The resulting method requires the simultaneous solution of the integral-momentum, moment-of-momentum and energy equations. It includes the ability to calculate nonequilibrium boundary-layer velocity profiles and also includes the modified Crocco-type relation for the temperature-velocity profile relation of reference 18. Although the present method is somewhat more complex than the initial version, as discussed previously, it still retains several simplifying assumptions, such as flat-plate friction, shear stress profile, and heat transfer, and no provision for a normal-pressure gradient. Also, all work to date has been limited to the perfect-gas regime of conventional aerodynamic wind tunnels, and the method has not been converted to real-gas relations. The effects of these assumptions are still under study, and the present version is considered interim in nature. The present method is used to predict distributions of displacement, momentum, and boundary-layer thickness along with velocity profiles.

SYMBOLS

A_1, A_2 constants of equation (12)

B constant in local shear relation (eq. (A21))

C function in equation (13) that depends on local integrated values of total energy and momentum deficiencies

c_f local friction coefficient, $\frac{\tau_w}{\rho_\delta u_\delta^2/2}$

c_p specific heat at constant pressure

D function defined by equation (A23)

E correlation function given by equation (B3)

F function given by equation (C4)

h static enthalpy

I constant in boundary-layer equation (I = 0 for two-dimensional flow; I = 1 for axisymmetric flow)

K parameter representing $\left(\kappa + \rho\kappa_e\right)$

M Mach number

N_{Pr} Prandtl number

p local static pressure

q_w heat transfer at wall

R Reynolds number

r body radius

s coordinate along body surface in direction of flow

T temperature

u local velocity parallel to body surface in direction of flow

v local velocity normal to body surface

w Cole's wake function

x	coordinate in free-stream direction
y	coordinate normal to body surface
Z	Karman function in modified Spalding-Chi heat transfer method of reference 6
δ	boundary-layer thickness
δ^*	displacement thickness
ϵ	eddy viscosity
θ	momentum thickness
κ	thermal conductivity
κ_e	eddy thermal conductivity
μ	viscosity
ρ	density
τ	local shear
φ	energy thickness
ω	angle between body surface coordinate and free-stream direction

Subscripts:

aw	adiabatic wall
i	inviscid
crit	point at which transition is assumed to begin
l	length of boundary-layer development

lam	laminar-boundary-layer value
t	stagnation value
tr	transitional-boundary-layer value
turb	turbulent-boundary-layer value
w	wall value
δ	boundary-layer-edge value
θ	based on momentum thickness
1,2	upstream and downstream stations, respectively

ANALYTICAL METHOD

Governing Equations

The flow of a compressible, viscous, heat-conducting fluid can be described by the continuity, Navier-Stokes, and energy equations. The boundary-layer equations may be derived from these equations for a viscous heat-conducting flow by substitution of mean and fluctuating parts for instantaneous flow variables, application of the Reynolds time-averaging process and, finally, neglecting higher-order terms (ref. 19). The resulting equations are valid for laminar, transitional, or turbulent boundary layers. If $(dp/dy)_w$ is assumed zero, and the body radius is assumed large relative to the boundary-layer thickness, the boundary-layer equations for two-dimensional or axisymmetric time steady flow are given by the following expressions:

Continuity:

$$\frac{\partial \rho u}{\partial s} + \frac{\partial \rho v}{\partial y} + \frac{I \rho u}{r} \frac{\partial r}{\partial s} = 0 \tag{1}$$

Momentum:

$$\rho u \frac{\partial u}{\partial s} + \rho v \frac{\partial u}{\partial y} = -\frac{\partial p}{\partial s} + \frac{\partial \tau}{\partial y} \tag{2}$$

Energy equation:

$$\rho u \frac{\partial h}{\partial s} + \rho v \frac{\partial h}{\partial y} = u \frac{\partial p}{\partial s} + \tau \frac{\partial u}{\partial y} + \frac{\partial}{\partial y}\left(\frac{K}{c_p} \frac{\partial h}{\partial y}\right) \tag{3}$$

where it is assumed that

$$\tau = (\mu + \rho\epsilon)\frac{\partial u}{\partial y} \tag{4}$$

and

$$K = \left(\kappa + \rho\kappa_e\right) \tag{5}$$

In the present method the continuity equation is combined with the momentum and energy equations and integrated across the boundary layer to produce integral forms for the momentum and energy equations. In addition to integral forms of the momentum and energy equations, another integral equation is generated by multiplying the momentum equation by the normal distance from the surface as a weighting function, combining the resulting equation with the continuity equation, and integrating across the boundary layer to form what is known as the integral moment-of-momentum equation. The details of the derivation of the integral-momentum, moment-of-momentum, and energy equations are given in appendix A where the assumption is made that $v_w = 0$. The integral equations are:

Integral-momentum equation:

$$\frac{d\theta}{dx} + \theta\left(\frac{2 + \frac{\delta^*}{\theta}}{u_\delta} \frac{du_\delta}{dx} + \frac{1}{\rho_\delta} \frac{d\rho_\delta}{dx} + \frac{I}{r} \frac{dr}{dx}\right) = \frac{1}{\cos \omega} \frac{\tau_w}{\rho_\delta u_\delta^2} = \frac{c_f}{2 \cos \omega} \tag{6}$$

Integral moment-of-momentum equation:

$$\frac{\delta_2}{\delta_1} = e^D \tag{7}$$

where

$$D = \frac{1}{3}\left\{\frac{Bc_f\,dx}{2\delta(B+1)\cos\omega\int_0^1 \frac{\rho u y}{\rho_\delta u_\delta \delta}\left(1-\frac{u}{u_\delta}\right)d\frac{y}{\delta}} - d\log_e \rho_\delta u_\delta^2 - d\log_e \int_0^1 \frac{\rho u y}{\rho_\delta u_\delta \delta}\left(1-\frac{u}{u_\delta}\right)d\frac{y}{\delta}\right.$$

$$- \frac{\int_0^1\left[\left(1-\frac{u}{u_\delta}\right)d\int_0^{y/\delta}\frac{\rho u}{\rho_\delta u_\delta}\,d\frac{y}{\delta}\right]d\frac{y}{\delta}}{\int_0^1 \frac{\rho u y}{\rho_\delta u_\delta \delta}\left(1-\frac{u}{u_\delta}\right)d\frac{y}{\delta}} - \left(d\log_e \rho_\delta u_\delta + I\,d\log_e r\right)\frac{\int_0^1\left[\left(1-\frac{u}{u_\delta}\right)\int_0^{y/\delta}\frac{\rho u}{\rho_\delta u_\delta}\,d\frac{y}{\delta}\right]d\frac{y}{\delta}}{\int_0^1 \frac{\rho u y}{\rho_\delta u_\delta \delta}\left(1-\frac{u}{u_\delta}\right)d\frac{y}{\delta}}$$

$$\left. - I\,d\log_e r - \frac{\left(1-2\int_0^1 \frac{\rho u y}{\rho_\delta u_\delta \delta}\,d\frac{y}{\delta}\right)d\log_e u_\delta}{2\int_0^1 \frac{\rho u y}{\rho_\delta u_\delta \delta}\left(1-\frac{u}{u_\delta}\right)d\frac{y}{\delta}}\right\}$$

Integral energy equation:

$$\frac{d\varphi}{dx} + \varphi\,\frac{d\log_e\left[\rho_\delta u_\delta\left(h_{t,\delta}-h_w\right)rI\right]}{dx} = \frac{q_w}{\cos\omega\rho_\delta u_\delta\left(h_{t,\delta}-h_w\right)} \tag{8}$$

In equations (6) to (8), the following equalities are assumed:

$$\int_0^\delta \frac{\rho u}{\rho_\delta u_\delta}\left(1-\frac{u}{u_\delta}\right)dy = \theta \tag{9}$$

$$\int_0^\delta \left(1-\frac{\rho u}{\rho_\delta u_\delta}\right)dy = \delta^* \tag{10}$$

and

$$\int_0^\delta \frac{\rho u}{\rho_\delta u_\delta}\left(\frac{h_{t,\delta}-h_t}{h_{t,\delta}-h_w}\right)dy = \varphi \tag{11}$$

where it has been assumed that the thermal-boundary-layer thickness equals the velocity-boundary-layer thickness.

The laminar-boundary-layer predictions presented herein were generated through the use of the similarity method of reference 13. However, any reliable laminar-boundary-layer method could be used as long as it gives values of the momentum thickness, the energy thickness, the laminar-boundary-layer friction coefficient, and the ratio

of momentum to boundary-layer thickness, all of which are needed at the point where transition is assumed to begin. The transitional- and turbulent-boundary-layer predictions presented were generated through the simultaneous solution of equations (6) to (8). Thus, the procedure followed when a complete boundary-layer solution (laminar, transitional, and turbulent) is desired consists of first obtaining a solution for the laminar region by use of an acceptable laminar boundary-layer method. Then, at the station where transition is assumed to begin, the transitional prediction method herein matches the laminar-boundary-layer parameters c_f, θ, θ/δ, and φ as obtained by the output of the laminar-boundary-layer program. The station at which transition begins has to be assumed but the end of transition, and thus the beginning of the turbulent region, is determined by the present method. The end of transition is taken to be the station where the computed transitional friction coefficient is 90 percent of the corresponding turbulent-friction coefficient. The turbulent-boundary-layer prediction then proceeds from this point to the end station of interest.

Auxiliary Relations for Turbulent-Boundary-Layer Solution

In order to obtain a simultaneous solution of equations (6) to (8) which is valid for turbulent boundary layers, auxiliary relations must be developed for the local-wall friction coefficient, the local-wall heat transfer, the boundary-layer velocity profiles, the boundary-layer temperature-velocity relation, and the shear distribution across the boundary layer. The flat-plate Spalding-Chi friction (based on R_θ) and the modified Spalding-Chi heat-transfer methods of references 20 and 21 are assumed to represent the local-wall friction and the local-wall heat transfer. In a positive pressure gradient the wall shear decreases from the Spalding-Chi value as the pressure gradient increases; therefore, the Spalding-Chi wall shear is the maximum possible wall shear in a positive pressure gradient.

A modified version of the equilibrium flat-plate log-log type velocity-profile relation of reference 22 is assumed to represent the boundary-layer velocity profile. The flat-plate boundary-layer velocity-profile relation of reference 22 was modified in order to approximate the pressure gradient effect on the velocity profile. The resulting velocity-profile relation is given by

$$\int_{u/u_\delta}^{1.0} \left(\frac{\rho}{\rho_\delta}\right)^{1/2} d\,\frac{u}{u_\delta} = A_1\left(\frac{c_f}{2}\right)^{1/2}\left(-A_2 \log_e \frac{y}{\delta} + 2 - w\right) \tag{12}$$

The parameter w is Cole's wake function as given in reference 23. Examination of equation (12) reveals that the term $A_2 \log_e \frac{y}{\delta}$ approaches zero as y/δ approaches 1.0 and the value of w approaches zero as y/δ approaches zero. Therefore, the term

$A_2 \log_e \frac{y}{\delta}$ becomes the dominant term as the wall is approached and w is dominant in the wake region. Examination of compressible turbulent-boundary-layer velocity profiles that have been distorted by pressure gradients revealed that the greatest effect on the local point values of velocity through the velocity profile is in the inner half of the profile. Therefore, for turbulent boundary layers the parameter A_1 is assumed to have a value of 1.25 as was the case for the equilibrium flat-plate velocity profiles of reference 22; and the parameter A_2 is an unknown that must be solved for in the solution of equations (6) to (8). For equilibrium flat-plate flow without heat transfer the value of the parameter A_2 as given in reference 22 is 2.0. It should be noted that the assumed velocity-profile relation does not give the correct linear variation next to the wall.

The modified Crocco-type temperature-velocity profile relation of reference 18 was used in the present boundary-layer-prediction method, as given by the following equation:

$$\frac{T}{T_\delta} = \frac{T_w}{T_\delta} + \left(1 - \frac{T_w}{T_\delta}\right)\left(\frac{u}{u_\delta}\right)^2 + \left[\frac{u}{u_\delta} - \left(\frac{u}{u_\delta}\right)^2\right]\frac{T_{aw} - T_w}{T_\delta}\frac{N_{Pr}}{Z} + C\left[\left(\frac{u}{u_\delta}\right)^2 - \left(\frac{u}{u_\delta}\right)^4\right] \tag{13}$$

The function Z is the Karman factor in the modified Spalding-Chi heat-transfer method of reference 21. The parameter C is a function of the local integrated total-energy and momentum deficiencies and is an unknown that must be determined in the solution of equations (6) to (8).

The relationship assumed for the shear distributions across the boundary layer was obtained by analytically fitting theoretical shear distributions derived (ref. 22) for flat-plate flow. The form of the analytical shear relation as developed for use in the present method is given by

$$\frac{\tau}{\tau_w} = 1 - \left(\frac{y}{\delta}\right)^B \tag{14}$$

A correlation of the parameter B was developed and is discussed in detail along with equation (14) in appendix B. The expression given in equation (14) monotonically decreases with distance from the wall, and therefore the τ_w value is the maximum shear in the profile. For all but severe pressure gradients the maximum shear occurs close to the surface and does not deviate a great deal from that for a zero pressure gradient (ref. 24). Therefore, a reasonably accurate shear integral for a pressure gradient case is obtained even though equation (14) does not give an accurate value of $(d\tau/dy)_w$ for this situation.

Auxiliary Relations for Transitional-Boundary-Layer Solution

As was the case for turbulent boundary layers, the solution of equations (6) to (8) for transitional boundary layers requires the assumption of auxiliary relations for the local-wall friction coefficient, the local-wall heat transfer, the boundary-layer velocity profiles, the boundary-layer temperature-velocity profiles, and the shear distribution across the boundary layer. These relations are discussed in appendix C.

Analytical Method of Solution

Substitution of the transitional or turbulent auxiliary relations into equations (6) to (8) produces three ordinary integral differential equations with three unknowns. The three unknowns consist of the parameter A_2 of the velocity profile, the parameter C of the temperature-velocity profile, and the boundary-layer thickness change. As is the case for most integral transitional- or turbulent-boundary-layer-prediction methods the present method requires values of several parameters at the initial station to begin the solution. The parameters which are required are the momentum thickness, the ratio of momentum to boundary-layer thickness, the energy thickness and, in the solutions which include a transition calculation, the value of the laminar friction coefficient. The resulting solution of equations (6) to (8) across a body surface element then consists in obtaining a first approximation of the values of A_2, C, and δ_2/δ_1 downstream of the element by use of the known parameters at the upstream station. Then, using successive approximations of the downstream values of the parameters A_2, C, and δ_2/δ_1 yields successively better average values over the element of the integral parameters δ^*, θ, φ, and the integral parameters of equation (8) are obtained and resubstituted into equations (6) to (8). This method of successive approximations is continued until two successive calculations produce a change in the downstream value of δ^* of $0.01\delta^*$ or less.

COMPARISONS OF THEORY AND EXPERIMENTAL DATA

The validity of the theoretical prediction procedure was tested by comparisons with experimental data. These comparisons also provide an indication of the range of applicability of the method since they cover a broad range of boundary conditions corresponding to a considerable quantity of experimental data. The experimental data were taken from references 17 and 25 to 29 and are presented in figures 1 to 10 in terms of boundary-layer velocity profiles and boundary-layer displacement and momentum-thickness distributions together with the corresponding theoretical computations. No comparisons between experimental and theoretical distributions of energy thickness are presented due to a lack of significant experimental results. The following discussion of these comparisons is divided into two general categories, axisymmetric and two-dimensional flow.

Two-Dimensional Flow

Comparisons between experiment and theory for the boundary-layer development on flat plates and two-dimensional compression surfaces are presented in figures 1 to 5 for a range of Mach numbers from 1.73 to 6.63 and ratios of wall temperature to free-stream stagnation temperature from 0.265 through adiabatic.

The experimental data of reference 27 presented in figure 1 consist of distributions of δ, δ^*, and θ along a flat plate for free-stream Mach numbers of 1.73, 2.0, and 2.5, and an adiabatic wall. The computation of the corresponding theoretical distributions of δ, δ^*, and θ, involved the use of two assumptions. A value of energy thickness of 0.01524 millimeter was assumed for the initial station, and the values of adiabatic wall temperature were determined by the following standard relation:

$$\frac{T_w}{T_\delta} = 1 + 0.896\left(\frac{1}{T_\delta/T_{t,\delta}} - 1\right) \tag{15}$$

The agreement between theory and experiment shown in figure 1 is within a few percent.

Experimental data from reference 28 and theoretical curves on the boundary-layer development in the constant-pressure region on a tunnel wall are given in figures 2 and 3 for Mach 3.0 and ratios of wall temperature to free-stream total temperature of 0.45, 0.65, and 0.85, and for Mach 6.0 and ratios of wall temperature to free-stream total temperature of 0.265 and 0.760, respectively. The experimental data of figure 4 were taken on a two-dimensional compression surface at Mach 6.0 with ratios of wall temperature to free-stream total temperature of 0.45 and 0.82 (ref. 28). The deviations between theoretical and experimental distributions of δ^* and θ for the flat-plate results of figures 2 and 3 are within the limits of data accuracy quoted by reference 28.

Because of the high wall curvatures of the Mach 6 two-dimensional isentropic compression surface of reference 28 and the large boundary-layer thicknesses, severe static-pressure gradients existed across the boundary layer normal to the wall. For the purposes of the present study, the presence of the normal-pressure gradient requires the experimental δ^* and θ to be defined in a slightly different manner than is usual in order to eliminate a normal-pressure-gradient contribution to the momentum and displacement thicknesses. The following definitions were assumed for δ^* and θ:

$$\delta^* = \int_0^\delta \left(1 - \frac{\rho u}{\rho_i u_i}\right) dy \tag{16}$$

$$\theta = \int_0^\delta \left(\frac{\rho u u_i}{\rho_i {u_i}^2} - \frac{\rho u^2}{\rho_i {u_i}^2}\right) dy \tag{17}$$

where $\rho_i u_i$, $\rho_i u_i^2$, u_i, ρu, and ρu^2 are based on the same local inviscid static-pressure distribution across the boundary layer. The subscripted i parameters are based on inviscid total pressures at the boundary-layer edge. The resulting δ^* and θ values thus obtained from the experimental data are to a first approximation a measure of the mass-flow deficiency and momentum deficiency of the boundary layer relative to the inviscid flow as caused by upstream surface friction losses. These definitions for δ^* and θ are consistent with those of the present theoretical method, which assumes constant static pressure across the boundary layer. Therefore, in an attempt to eliminate any static-pressure contributions to experimental values of δ^* and θ, the slightly modified definitions of δ^* and θ as given in equations (16) and (17) were used to reduce the experimental data. Reference 28 presented distributions of wall static pressure and boundary-layer-edge static pressure along the compression surface. A linear distribution of static pressure between the wall value and the boundary-layer-edge value was assumed in the reduction of the experimental data. The comparisons of figure 4 indicate a reasonable agreement between experimental and theoretically predicted trends of δ, δ^*, and θ.

Experimental data from reference 29 are presented in figure 5 for the boundary-layer development on a cooled flat plate which spanned the tunnel test section. The data cover a range of Mach number from 6.22 to 6.54 and a range of ratios of wall temperature to free-stream total temperature from 0.46 to 0.83, as noted in the individual parts of this figure. From figures 20 and 21 of reference 29 it is estimated that the repeatability of experimental values of θ is within approximately ±6.5 percent and the repeatability of experimental values of δ^* is within approximately ±15.7 percent. The differences between the experimental and theoretical distributions of δ^* and θ of figure 5 in most cases are also within these repeatability limits.

Axisymmetric Flow

Theoretical and experimental data are presented in figures 6 and 7 for the investigation described in reference 17 on the boundary-layer development on a cooled axisymmetric body of revolution at a free-stream Mach number of 4.0. In general, the test body up to the survey station consisted of a blunted 10.25° half-angle cone followed by 11.15° of isentropic compression followed by 6° to 7° of expansion. (See fig. 6.) Experimental static- and total-pressure surveys were conducted normal to the test body axis at the 344.5-millimeter (from cone vertex) axial location for ratios of wall temperature to free-stream total temperature of 0.2, 0.7, and 0.9. The experimental values of displacement thickness and momentum thickness were computed from the experimental surveys by assuming a temperature-velocity profile corresponded to the relation of equation (13). The theoretical distributions of δ, δ^*, and θ presented on figure 6 were generated by using the present theoretical method along with the assumption that transition from a laminar to a turbulent boundary layer began at the trips (44.6 millimeters from cone

vertex). Boundary-layer-edge Mach numbers and static pressures along the test body were determined through use of the blunt body and characteristic theories of references 30 to 32. The boundary-layer computation through transition was initiated using the results from an altered version of the laminar-similarity-type computer solution of reference 13. No correction for trip losses was included in the computational procedure. The analytical and experimental results of figure 6 indicate agreement within ±6.8 percent for the momentum thickness, within ±5.3 percent for the displacement thickness, and within ±9 percent for the boundary-layer thickness. In general, the present method, with the provision for nonequilibrium velocity profiles, predicted values of θ and δ^* slightly more accurately than the initial version used in reference 17; however, substantial improvements in the accuracy of the prediction of boundary-layer thickness δ were obtained by use of the present method since the prediction error for δ in reference 17 was approximately -40 percent. This effect is illustrated further by the velocity-distribution comparisons of figure 7, which indicate close agreement except for a region adjacent to the surface ranging from 2 to 6 percent of the boundary-layer thickness, where the laminar sublayer was not predicted.

The values of theoretical and experimental parameters agree very closely (figs. 6 and 7) considering that the boundary-layer-trip losses were neglected in the theoretical computations. In order to explore this result further, boundary-layer computations for the temperature ratio of 0.9 case were made for several initial values of θ and $c_{f,lam}$. These results are presented in figure 8. As a reference, the curve from figure 6(c) for no-trip correction is also shown.

In figure 8 the distributions of momentum thickness shown by cases 1 and 2 were obtained by increasing the initial momentum thickness by 79 and 143 percent, respectively, over the no-trip correction case, while the laminar friction coefficient assumed at the beginning of transition was held constant. This drastic increase in initial momentum thickness resulted in a shift of the axial location of the end of transition from about 180 millimeters for the no-trip correction case, to about 240 millimeters for case 1, and about 271 millimeters for case 2. The variation of the predicted momentum thickness at the survey station was only about 2 percent; similar small variations were obtained for predicted values of displacement and boundary-layer thicknesses at the survey station. The effect of reducing the friction coefficient (17 percent decrease) at the start of transition while simultaneously increasing the momentum thickness (143 percent increase) is shown by case 3, figure 8. For case 3 the end of transition occurred beyond the survey station and the momentum thickness at the survey station was reduced by 17 percent.

Additional data on the boundary-layer development on axisymmetric bodies are given in reference 25 for a free-stream Mach number of 5.98 and an adiabatic wall. The test body in this case consisted of an initial 10° half-angle sharp cone followed by approximately 25.4° of isentropic compression. Two sets of theoretical curves and experimental

data from the investigation are shown on figure 9; one set was computed by the present turbulent boundary-layer-prediction method, and the other set was computed by the same prediction method but altered by the assumption of equilibrium flat-plate velocity profiles. For these computations the boundary-layer-edge Mach number distribution was assumed to be that for the 10° cone case presented in figure 6 of reference 25, and the boundary-layer-edge static pressures are assumed to correspond to the edge Mach numbers assumed and the total-pressure recovery through the conical shock. Figure 9 shows that the assumption of flat-plate velocity profiles has only a small effect on δ^* and θ but considerably underpredicts the boundary-layer thickness δ. The assumption of nonequilibrium profiles of the present method predicts the boundary-layer thickness and its development within approximately ±14 percent. From the results presented herein and also in reference 17, it is concluded that the prediction of boundary-layer growth in either positive or negative pressure gradients requires a provision for nonequilibrium velocity profiles in the theoretical method.

Experimental data on another type of axisymmetric body are reported in reference 26 and presented in figure 10. The experimental data of figures 10(a) and 10(b) were generated on a body consisting of 431.8 millimeters of open cylinder followed by a 482.2 millimeters of isentropic compression surface which turns the flow 35.6°. These data were taken at free-stream Mach numbers of 5 and 6 with no wall cooling. The experimental data of figures 10(c) and 10(d) were generated on cooled bodies consisting of an open cylinder followed by a compression surface 934 millimeters in length which turned the flow isentropically by 34.4°. The data of figure 10(c) correspond to Mach 6 and an open-cylinder length of 304.9 millimeters; the data of figure 10(d) correspond to Mach 8 and a cylinder length of 660.4 millimeters. In figure 10(c) the experimental data points for boundary-layer thickness connected by the lines indicate the believed reading accuracy for the experimental boundary-layer thicknesses.

In these experimental investigations boundary-layer surveys (ref. 26) were conducted normal to the wall for static pressure, pitot pressure, and total temperature. In the data-reduction procedure of reference 26, static pressures across the boundary layer were assumed to correspond to those computed inviscidly because the measured static pressure were not sufficiently accurate. Because of the large boundary-layer thicknesses relative to the axisymmetric body's radius and surface curvature, a significant amount of static-pressure gradient normal to the body surface is present in the experimental data. Therefore, in an attempt to eliminate any static-pressure contributions to the experimental δ^* and θ the slightly modified definitions of δ^* and θ as given in equations (16) and (17) were again used to reduce the experimental data. When the definitions for the experimental δ^* and θ as given by equations (16) and (17) were used, the present theoretical turbulent-boundary-layer method was found to predict trends of the

development of the displacement, momentum, and boundary-layer thicknesses reasonably well for all the sample experimental cases (fig. 10).

CONCLUDING REMARKS

In connection with research programs on hypersonic airbreathing propulsion, an integral method for predicting boundary-layer development in transition and turbulent-flow regions on two-dimensional or axisymmetric bodies has been developed through use of the integral-momentum, moment-of-momentum, and energy equations together with appropriate auxiliary equations. The method has the capability of predicting nonequilibrium velocity distributions. It employs some simplifying assumptions, such as flat-plate friction and heat-transfer coefficients, no provision for a normal-pressure gradient, and perfect-gas relations; therefore, the method is considered interim in nature.

Extensive comparisons have been made with data covering a wide Mach number range, cooled and uncooled walls, two-dimensional and axisymmetric bodies with and without regions of longitudinal-pressure gradient, and a few cases with strong normal-pressure gradients. The overall conclusion is that the method will predict the displacement, momentum, and boundary-layer thickness of the data within the limits of the experimental accuracy.

Langley Research Center,
National Aeronautics and Space Administration,
Hampton, Va., June 15, 1971.

APPENDIX A

THEORETICAL DERIVATION OF INTEGRAL FORMS OF GOVERNING EQUATIONS

In the derivation of the integral forms of the governing boundary-layer equations, consider the following equations:

Continuity equation:

$$\frac{\partial \rho u}{\partial s} + \frac{\partial \rho v}{\partial y} + \frac{I \rho u}{r} \frac{\partial r}{\partial s} = 0 \tag{A1}$$

Momentum equation:

$$\rho u \frac{\partial u}{\partial s} + \rho v \frac{\partial u}{\partial y} = -\frac{\partial p}{\partial s} + \frac{\partial \tau}{\partial y} \tag{A2}$$

Multiply equation (A1) by $\left(u_\delta - u\right)$ to obtain

$$\left(u_\delta - u\right)\frac{\partial \rho u}{\partial s} + \left(u_\delta - u\right)\frac{\partial \rho v}{\partial y} + \frac{I \rho u}{r}\left(u_\delta - u\right)\frac{\partial r}{\partial s} = 0 \tag{A3}$$

Substract equation (A2) from equation (A3) to obtain

$$\left(u_\delta - u\right)\frac{\partial \rho u}{\partial s} - \rho u \frac{\partial u}{\partial s} + \left(u_\delta - u\right)\frac{\partial \rho v}{\partial y} - \rho v \frac{\partial u}{\partial y} + \frac{I \rho u}{r}\left(u_\delta - u\right)\frac{\partial r}{\partial s} = \frac{\partial p}{\partial s} - \frac{\partial \tau}{\partial y} \tag{A4}$$

Rearrangement of equation (A4) gives:

$$\frac{\partial}{\partial s}\left[\rho u\left(u_\delta - u\right)\right] + \frac{\partial}{\partial y}\left[\rho v\left(u_\delta - u\right)\right] - \rho u \frac{\partial u_\delta}{\partial s} + \rho u\left(u_\delta - u\right)\frac{I}{r}\frac{\partial r}{\partial s} = \frac{\partial p}{\partial s} - \frac{\partial \tau}{\partial y}$$

or

$$\rho_\delta u_\delta^2 \frac{\partial}{\partial s}\left[\frac{\rho u}{\rho_\delta u_\delta}\left(1 - \frac{u}{u_\delta}\right)\right] + \frac{\partial}{\partial y}\left[\rho v\left(u_\delta - u\right)\right] + \left[\frac{\rho u}{\rho_\delta u_\delta}\left(1 - \frac{u}{u_\delta}\right)\right]\left(u_\delta^2 \frac{\partial \rho_\delta}{\partial s} + 2 u_\delta \rho_\delta \frac{\partial u_\delta}{\partial s}\right) - \rho u \frac{\partial u_\delta}{\partial s}$$

$$+ \rho u\left(u_\delta - u\right)\frac{I}{r}\frac{\partial r}{\partial s} = \frac{\partial p}{\partial s} - \frac{\partial \tau}{\partial y} \tag{A5}$$

But with isentropic flow at the boundary-layer edge,

$$\frac{\partial p}{\partial s} = -\rho_\delta u_\delta \frac{\partial u_\delta}{\partial s} \tag{A6}$$

Substitution of equation (A6) into equation (A5) and integrating with respect to y gives, after rearrangement, the integral-momentum equation

$$\frac{d\theta}{dx} + \theta\left(\frac{2 + \frac{\delta^*}{\theta}}{u_\delta}\frac{du_\delta}{dx} + \frac{1}{\rho_\delta}\frac{d\rho_\delta}{dx} + \frac{I}{r}\frac{dr}{dx}\right) = \frac{1}{\cos\omega}\frac{\tau_w}{\rho_\delta u_\delta^2} = \frac{c_f}{2\cos\omega} \tag{A7}$$

where

$$\int_0^\delta \frac{\partial}{\partial y}\rho v\left(u_\delta - u\right)dy = 0 \tag{A8}$$

$$\int_0^\delta \frac{\rho u}{\rho_\delta u_\delta}\left(1 - \frac{u}{u_\delta}\right)dy = \theta \tag{A9}$$

$$\int_0^\delta \left(1 - \frac{\rho u}{\rho_\delta u_\delta}\right)dy = \delta^* \tag{A10}$$

and

$$ds = \frac{dx}{\cos\omega} \tag{A11}$$

where ω is the surface angle relative to the axis of symmetry in axisymmetric flow and the angle of the surface relative to the initial station surface plane in two-dimensional flow.

Multiply equations (A3) and (A1) by y to obtain

$$y\left(u_\delta - u\right)\frac{\partial \rho u}{\partial s} + y\left(u_\delta - u\right)\frac{\partial \rho v}{\partial y} + \frac{I\rho u y}{r}\left(u_\delta - u\right)\frac{\partial r}{\partial s} = 0 \tag{A12}$$

$$y\rho u\frac{\partial u}{\partial s} + y\rho v\frac{\partial u}{\partial y} = -y\frac{\partial p}{\partial s} + y\frac{\partial \tau}{\partial y} \tag{A13}$$

Subtracting equation (A13) from equation (A12) and rearranging gives

$$-\rho v(u_\delta - u) + \frac{\partial}{\partial s}\left[y\rho u(u_\delta - u)\right] + \frac{\partial}{\partial y}\left[y\rho v(u_\delta - u)\right]$$
$$- \rho uy \frac{\partial u_\delta}{\partial s} + \rho uy(u_\delta - u)\frac{I}{r}\frac{\partial r}{\partial s} = y\frac{\partial p}{\partial s} - y\frac{\partial \tau}{\partial y} \qquad (A14)$$

Substitution of equations (A6) and (A11) into equation (A14) and integrating with respect to y gives, after rearrangement,

$$-\frac{1}{\cos\omega}\int_0^\delta \rho v(u_\delta - u)dy + \frac{d}{dx}\int_0^\delta \rho uy(u_\delta - u)dy - \frac{du_\delta}{dx}\int_0^\delta \rho uy\, dy + \frac{I}{r}\frac{dr}{dx}\int_0^\delta \rho uy(u_\delta - u)dy$$
$$= -\frac{\delta^2}{2}\rho_\delta u_\delta \frac{du_\delta}{dx} - \frac{1}{\cos\omega}\int_0^\delta y\frac{\partial \tau}{\partial y}dy \qquad (A15)$$

where

$$\int_0^\delta \frac{\partial}{\partial y}\left[y\rho v(u_\delta - u)\right]dy = 0 \qquad (A16)$$

Through use of the continuity equation,

$$\frac{1}{\cos\omega}\int_0^\delta \rho v(u_\delta - u)dy = -\int_0^\delta (u_\delta - u)\frac{d\int_0^y \rho u\, dy}{dx}dy - \frac{I}{r}\frac{dr}{dx}\int_0^\delta\left[(u_\delta - u)\int_0^y \rho u\, dy\right]dy \qquad (A17)$$

or

$$\frac{1}{\cos\omega}\int_0^\delta \rho v(u_\delta - u)dy = -\rho_\delta u_\delta^2\delta^2\int_0^1\left[\left(1 - \frac{u}{u_\delta}\right)\frac{d\int_0^{y/\delta}\frac{\rho u}{\rho_\delta u_\delta}d\frac{y}{\delta}}{dx}\right]d\frac{y}{\delta}$$
$$- u_\delta\delta^2\left(\frac{d\rho_\delta u_\delta}{dx} + \frac{I\rho_\delta u_\delta}{r}\frac{dr}{dx}\right)\int_0^1\left[\left(1 - \frac{u}{u_\delta}\right)\int_0^{y/\delta}\frac{\rho u}{\rho_\delta u_\delta}d\frac{y}{\delta}\right]d\frac{y}{\delta}$$
$$- \rho_\delta u_\delta^2\delta\frac{d\delta}{dx}\int_0^1\left(1 - \frac{u}{u_\delta}\right)\frac{\rho uy}{\rho_\delta u_\delta\delta}d\frac{y}{\delta} \qquad (A18)$$

Substitution of equation (A18) into equation (A15) gives, after rearrangement,

$$\int_0^1 \frac{\rho u y}{\rho_\delta u_\delta \delta}\left(1 - \frac{u}{u_\delta}\right) d\frac{y}{\delta} \frac{d\rho_\delta {u_\delta}^2 \delta^2}{dx} + \rho_\delta {u_\delta}^2 \delta^2 \frac{d}{dx}\left[\int_0^1 \frac{\rho u y}{\rho_\delta u_\delta \delta}\left(1 - \frac{u}{u_\delta}\right) d\frac{y}{\delta}\right]$$

$$+ \rho_\delta {u_\delta}^2 \delta^2 \int_0^1 \left(1 - \frac{u}{u_\delta}\right) \frac{d\int_0^{y/\delta} \frac{\rho u}{\rho_\delta u_\delta} d\frac{y}{\delta}}{dx} d\frac{y}{\delta} + {u_\delta}^2 \delta^2 \left(\frac{d\rho_\delta u_\delta}{dx} + \frac{I \rho_\delta u_\delta}{r}\frac{dr}{dx}\right)$$

$$\times \int_0^1 \left[\left(1 - \frac{u}{u_\delta}\right) \int_0^{y/\delta} \frac{\rho u}{\rho_\delta u_\delta} d\frac{y}{\delta}\right] d\frac{y}{\delta} + \rho_\delta {u_\delta}^2 \delta \frac{d\delta}{dx} \int_0^1 \left(1 - \frac{u}{u_\delta}\right) \frac{\rho u y}{\rho_\delta u_\delta \delta} d\frac{y}{\delta}$$

$$- \rho_\delta u_\delta \delta^2 \frac{du_\delta}{dx} \int_0^1 \frac{\rho u y}{\rho_\delta u_\delta \delta} d\frac{y}{\delta} + \rho_\delta {u_\delta}^2 \delta^2 \frac{I}{r}\frac{dr}{dx} \int_0^1 \frac{\rho u y}{\rho_\delta u_\delta \delta}\left(1 - \frac{u}{u_\delta}\right) d\frac{y}{\delta}$$

$$= -\frac{\delta^2}{2} \rho_\delta u_\delta \frac{du_\delta}{dx} - \frac{\delta}{\cos \omega} \int_0^1 \frac{y}{\delta} \frac{\partial \tau}{\partial \frac{y}{\delta}} d\frac{y}{\delta} \qquad \text{(A19)}$$

Dividing through by

$$\rho_\delta {u_\delta}^2 \delta^2 \int_0^1 \frac{\rho u y}{\rho_\delta u_\delta \delta}\left(1 - \frac{u}{u_\delta}\right) d\frac{y}{\delta}$$

and rearranging gives

$$\frac{d}{dx} \log_e \rho_\delta {u_\delta}^2 \delta^2 + \frac{d}{dx} \log_e \int_0^1 \frac{\rho u y}{\rho_\delta u_\delta \delta}\left(1 - \frac{u}{u_\delta}\right) d\frac{y}{\delta} + \frac{\int_0^1 \left[\left(1 - \frac{u}{u_\delta}\right) \frac{d}{dx} \int_0^{y/\delta} \frac{\rho u}{\rho_\delta u_\delta} d\frac{y}{\delta}\right] d\frac{y}{\delta}}{\int_0^1 \frac{\rho u y}{\rho_\delta u_\delta \delta}\left(1 - \frac{u}{u_\delta}\right) d\frac{y}{\delta}}$$

$$+ \left(\frac{d \log_e \rho_\delta u_\delta}{dx} + \frac{I}{r}\frac{dr}{dx}\right) \frac{\int_0^1 \left[\left(1 - \frac{u}{u_\delta}\right) \int_0^{y/\delta} \frac{\rho u}{\rho_\delta u_\delta} d\frac{y}{\delta}\right] d\frac{y}{\delta}}{\int_0^1 \frac{\rho u y}{\rho_\delta u_\delta \delta}\left(1 - \frac{u}{u_\delta}\right) d\frac{y}{\delta}} + \frac{d \log_e \delta}{dx} + I \frac{d \log_e r}{dx}$$

(Equation continued on next page)

$$+\frac{1-2\int_0^1 \frac{\rho u y}{\rho_\delta u_\delta \delta}\,d\frac{y}{\delta}}{2\int_0^1 \frac{\rho u y}{\rho_\delta u_\delta \delta}\left(1-\frac{u}{u_\delta}\right)d\frac{y}{\delta}}\,\frac{d\log_e u_\delta}{dx}=-\frac{1}{\rho_\delta u_\delta{}^2\delta\cos\omega}\,\frac{\int_0^1 \frac{y}{\delta}\frac{d\tau}{d\frac{y}{\delta}}\,d\frac{y}{\delta}}{\int_0^1 \frac{\rho u y}{\rho_\delta u_\delta \delta}\left(1-\frac{u}{u_\delta}\right)d\frac{y}{\delta}} \tag{A20}$$

The relationship assumed for the shear distribution across the boundary layer and discussed in detail in appendix B is given by

$$\frac{\tau}{\tau_w}=1-\left(\frac{y}{\delta}\right)^B \tag{A21}$$

Substitution of equation (A21) into equation (A20) and rearrangement of the results gives the integral moment-of-momentum equation:

$$\frac{\delta_2}{\delta_1}=e^D \tag{A22}$$

where

$$D=\frac{1}{3}\left\{\frac{Bc_f\,dx}{2\delta(B+1)\cos\omega\int_0^1 \frac{\rho u y}{\rho_\delta u_\delta \delta}\left(1-\frac{u}{u_\delta}\right)d\frac{y}{\delta}}-d\log_e\rho_\delta u_\delta{}^2-d\log_e\int_0^1 \frac{\rho u y}{\rho_\delta u_\delta \delta}\left(1-\frac{u}{u_\delta}\right)d\frac{y}{\delta}\right.$$

$$-\frac{\int_0^1\left[\left(1-\frac{u}{u_\delta}\right)d\int_0^{y/\delta}\frac{\rho u}{\rho_\delta u_\delta}\,d\frac{y}{\delta}\right]d\frac{y}{\delta}}{\int_0^1 \frac{\rho u y}{\rho_\delta u_\delta \delta}\left(1-\frac{u}{u_\delta}\right)d\frac{y}{\delta}}-\left(d\log_e\rho_\delta u_\delta+I\,d\log_e r\right)$$

$$\left.\times\frac{\int_0^1\left[\left(1-\frac{u}{u_\delta}\right)\int_0^{y/\delta}\frac{\rho u}{\rho_\delta u_\delta}\,d\frac{y}{\delta}\right]d\frac{y}{\delta}}{\int_0^1 \frac{\rho u y}{\rho_\delta u_\delta \delta}\left(1-\frac{u}{u_\delta}\right)d\frac{y}{\delta}}-I\,d\log_e r-\frac{\left(1-2\int_0^1 \frac{\rho u y}{\rho_\delta u_\delta \delta}\,d\frac{y}{\delta}\right)d\log_e u_\delta}{2\int_0^1 \frac{\rho u y}{\rho_\delta u_\delta \delta}\left(1-\frac{u}{u_\delta}\right)d\frac{y}{\delta}}\right\} \tag{A23}$$

The energy equation, as previously noted in equation (3), is

$$\rho u\frac{\partial h}{\partial s}+\rho v\frac{\partial h}{\partial y}=u\frac{\partial p}{\partial s}+\tau\frac{\partial u}{\partial y}+\frac{\partial}{\partial y}\left(\frac{K}{c_p}\frac{\partial h}{\partial y}\right) \tag{A24}$$

Stagnation enthalpy is given by

$$h_t = h + \frac{u^2}{2} \tag{A25}$$

and thus,

$$\left.\begin{aligned} \frac{\partial h}{\partial s} &= \frac{\partial h_t}{\partial s} - u\frac{\partial u}{\partial s} \\ \frac{\partial h}{\partial y} &= \frac{\partial h_t}{\partial y} - u\frac{\partial u}{\partial y} \end{aligned}\right\} \tag{A26}$$

Substitution of equations (A26) into equation (A24) gives

$$\rho u\frac{\partial h_t}{\partial s} - \rho u^2\frac{\partial u}{\partial s} + \rho v\frac{\partial h_t}{\partial y} - \rho v u\frac{\partial u}{\partial y} = u\frac{\partial p}{\partial s} + \tau\frac{\partial u}{\partial y} + \frac{\partial}{\partial y}\left(\frac{K}{c_p}\frac{\partial h}{\partial y}\right) \tag{A27}$$

Multiply equation (A1) by $\left(h_{t,\delta} - h_t\right)$ to obtain

$$\left(h_{t,\delta} - h_t\right)\frac{\partial \rho u}{\partial s} + \left(h_{t,\delta} - h_t\right)\frac{\partial \rho v}{\partial y} + \left(h_{t,\delta} - h_t\right)\frac{\rho u I}{r}\frac{\partial r}{\partial s} = 0 \tag{A28}$$

Subtracting equation (A27) from equation (A28) gives

$$\left(h_{t,\delta} - h_t\right)\frac{\partial \rho u}{\partial s} + \left(h_{t,\delta} - h_t\right)\frac{\partial \rho v}{\partial y} + \left(h_{t,\delta} - h_t\right)\frac{\rho u I}{r}\frac{\partial r}{\partial s} - \rho u\frac{\partial h_t}{\partial s} + \rho u^2\frac{\partial u}{\partial s} - \rho v\frac{\partial h_t}{\partial y} + \rho v u\frac{\partial u}{\partial y}$$

$$= -u\frac{\partial p}{\partial s} - \tau\frac{\partial u}{\partial y} - \frac{\partial}{\partial y}\left(\frac{K}{c_p}\frac{\partial h}{\partial y}\right) \tag{A29}$$

Substitution of equation (A2) into equation (A29) (for terms 5 and 7) gives, after rearrangement,

$$\frac{\partial\left[\rho u\left(h_{t,\delta} - h_t\right)\right]}{\partial s} + \frac{\partial\left[\rho v\left(h_{t,\delta} - h_t\right)\right]}{\partial y} - u\frac{\partial p}{\partial s} + u\frac{\partial \tau}{\partial y} + \left(h_{t,\delta} - h_t\right)\frac{\rho u I}{r}\frac{dr}{ds} = u\frac{\partial p}{\partial s} - \tau\frac{\partial u}{\partial y} - \frac{\partial}{\partial y}\left(\frac{K}{c_p}\frac{\partial h}{\partial y}\right) \tag{A30}$$

Integrating equation (A30) with respect to y gives

$$\frac{d}{ds}\int_0^\delta \rho u\left(h_{t,\delta} - h_t\right)dy + \frac{I}{r}\frac{dr}{ds}\int_0^\delta \rho u\left(h_{t,\delta} - h_t\right)dy = q_w \tag{A31}$$

where

$$\left.\begin{aligned}\int_0^\delta \frac{\partial \rho v\left(h_{t,\delta} - h_t\right)}{\partial y}\,dy = 0\\ \int_0^\delta \frac{\partial (u\tau)}{\partial y}\,dy = 0\end{aligned}\right\} \tag{A32}$$

$$\int_0^\delta \frac{\partial}{\partial y}\left(\frac{K}{c_p}\frac{\partial h}{\partial y}\right)dy = \left(\frac{K}{c_p}\frac{\partial h}{\partial y}\right)_w \tag{A33}$$

and the heat transfer at the wall is

$$q_w = \left(\frac{K}{c_p}\frac{\partial h}{\partial y}\right)_w \tag{A34}$$

Substituting

$$\varphi = \int_0^\delta \frac{\rho u}{\rho_\delta u_\delta}\left(\frac{h_{t,\delta} - h_t}{h_{t,\delta} - h_w}\right)dy \tag{A35}$$

and equation (A11) into equation (A31) and rearranging yields the integral energy equation:

$$\frac{d\varphi}{dx} + \varphi\,\frac{d\,\log_e\left[\rho_\delta u_\delta\left(h_{t,\delta} - h_w\right)r^I\right]}{dx} = \frac{q_w}{\cos\,\omega\rho_\delta u_\delta\left(h_{t,\delta} - h_w\right)} \tag{A36}$$

APPENDIX B

SHEAR STRESS INTEGRAL

The two-dimensional, compressible, turbulent-boundary-layer equations for steady mean flow along a flat plate were integrated numerically from the wall to various positions within the boundary layer, yielding the turbulent-shear-stress profile, and some sample results are presented in reference 13. An equation of the following form was found to give an analytical fit to the sample shear distributions presented in reference 13:

$$\frac{\tau}{\tau_w} = 1 - \left(\frac{y}{\delta}\right)^B \tag{B1}$$

An analytical correlation of the parameter B for adiabatic equilibrium flat-plate turbulent boundary layers has been developed in such a manner as to be applicable to nonequilibrium boundary layers. This correlation was accomplished in the following manner.

For adiabatic equilibrium flat-plate flow the parameter A_2 of the turbulent-velocity-profile relation of equation (12) has a constant value of 2.0. Therefore, substitution of the turbulent auxiliary relationships into equations (6) to (8) and assuming the velocity-profile parameter A_2 to be 2.0 produces a set of three integral differential equations with three unknowns, B, C, and δ. The resulting integral differential equations were then solved for a range of boundary-layer-edge Mach numbers and Reynolds numbers R_θ. The solutions for the parameter B revealed that an increase in the value of B causes an increase in the entrainment of free-stream mass flow to the boundary layer. The increase in mass entrainment with an increase in the value of B suggested that the parameter B should be correlated with a characteristic of the velocity profile near the boundary-layer edge. The following expression is therefore obtained for the correlation of B:

$$\frac{B}{B+1} = 0.08534 \log_e E + 0.7955 \tag{B2}$$

where

$$E = M_\delta^2 \left[\frac{d\left(\frac{1}{T} d\frac{u}{u_\delta}\right)^2}{T_\delta \, d\frac{y}{\delta}} \right]_{d\frac{y}{\delta}} \Bigg]_{\frac{y}{\delta}=0.95} \tag{B3}$$

It is assumed that resulting correlation can also be applied in the computation of transitional and nonequilibrium-type boundary layers. The reasoning on which this assumption is based resulted from a comparison of nonequilibrium-type velocity profiles in the constant-pressure region downstream of a shock-boundary-layer interaction with those for equilibrium flow. This comparison reveals a strong similarity in shape between the nonequilibrium velocity profiles and the equilibrium velocity profiles for much smaller Reynolds numbers. Based on this observation as to the relative similarity of the velocity-profile shapes, the assumption was made that the shear distributions would also be similar in shape. Thus, it is assumed that the correlation of the parameter B in terms of a characteristic of the velocity profile, as has been done for adiabatic equilibrium flat-plate turbulent boundary layers (eqs. (B2) and (B3)), can be applied to transitional and nonequilibrium turbulent boundary layers.

APPENDIX C

AUXILIARY RELATIONS FOR TRANSITIONAL BOUNDARY-LAYER SOLUTION

On page 434 of reference 19, the variation of the local-wall friction coefficient through the transition region is expressed by

$$c_{f,tr} = c_{f,turb} - \frac{R_{l,crit}}{R_l}\left(c_{f,turb} - c_{f,lam}\right)_{crit} \tag{C1}$$

The Reynolds numbers $R_{l,crit}$ and R_l are based on the length of boundary-layer development. The subscript crit refers to the point at which transition is assumed to begin. The Reynolds number based on momentum thickness is used to compute the local-friction coefficient since even in a zero-pressure-gradient region the friction coefficient based on length of boundary-layer development is not valid after a pressure gradient. Also, one main problem exists in the use of equation (C1) to represent the distribution of the friction coefficient through the transition region. This problem results from the fact that in a pressure gradient the value of the ratio of $R_{l,crit}$ and R_l can change drastically and cause equation (C1) to produce erroneous transition friction coefficients (possibly less than the corresponding local laminar friction coefficient based on R_θ). To eliminate this problem the following relationship is assumed for the distribution of the friction coefficient through the transition region:

$$c_{f,tr} = c_{f,turb} - \frac{c_{f,turb}}{R_\theta}\left[R_\theta \frac{\left(c_{f,turb} - c_{f,lam}\right)}{c_{f,turb}}\right]_{crit} \tag{C2}$$

The method of scaling the value of $\left(c_{f,turb} - c_{f,lam}\right)_{crit}$ expressed in equation (C2) produces a reasonable distribution of friction coefficient through the transition region.

As is done in the turbulent-boundary-layer region, the heat transfer in the transition region is computed by using the modified Spalding-Chi heat-transfer method for turbulent flow (ref. 21). This relation overpredicts the heat transfer in the transition region but was selected as a matter of convenience since the total heat load in the transition region is small for practical configurations.

The velocity-profile relation of equation (12) which was used for the turbulent region was also assumed to apply in the transitional-boundary-layer region. Examination of experimental laminar- and transitional-boundary-layer velocity profiles revealed that the

profiles are steeper than those of turbulent flow. An increase in the value of A_1 produces a similar effect in equation (12). A value of A_1 of 2.5 used in equation (12) resulted in predicted velocity profiles similar in shape to those of a laminar boundary layer. Consequently, the parameter A_1 was allowed to vary through the transition region in the manner given by the following equation:

$$A_1 = \frac{1.25\left(c_{f,turb} - c_{f,tr}\right)}{\left(c_{f,turb} - c_{f,lam}\right)_{crit}} + 1.25 \tag{C3}$$

The temperature-velocity profile relation of equation (13) for turbulent flow was altered for use in the transitional-boundary-layer region in a manner such that the slope of the temperature-velocity profile at the body surface is between that for a turbulent boundary layer and that for a laminar boundary layer. Therefore, through transition the slope of the temperature-velocity profile at the surface is assumed to be given by

$$F = \left[\frac{c_{f,tr} - c_{f,turb}}{\left(c_{f,turb} - c_{f,lam}\right)_{crit}}\right]\left\{\frac{\left[\left(\frac{T_{aw}}{T_\delta}\right)_{turb} - \frac{T_w}{T_\delta}\right]0.725}{Z} - \left[\left(\frac{T_{aw}}{T_\delta}\right)_{lam} - \frac{T_w}{T_\delta}\right]0.725^{1/3}\right\} + \left[\left(\frac{T_{aw}}{T_\delta}\right)_{turb} - \frac{T_w}{T_\delta}\right]\frac{0.725}{Z} \tag{C4}$$

where Z is the Karman factor of reference 21. In the transition region, equation (13) for the temperature-velocity profile relation becomes

$$\frac{T}{T_\delta} = \frac{T_w}{T_\delta} + \left(1 - \frac{T_w}{T_\delta}\right)\left(\frac{u}{u_\delta}\right)^2 + \left[\frac{u}{u_\delta} - \left(\frac{u}{u_\delta}\right)^2\right]F + C\left[\left(\frac{u}{u_\delta}\right)^2 - \left(\frac{u}{u_\delta}\right)^4\right] \tag{C5}$$

Through the transitional-boundary-layer region the shear distribution across the boundary layer is assumed to be given by equation (14) for lack of a more appropriate expression. Thus, numerical values of several parameters in the transition region are based on weighted values of friction coefficients and others are assumed to be the same as for turbulent flow, as discussed. This procedure is somewhat arbitrary but does provide a systematic method for computing a finite transition length, which is the primary objective in the present method.

In summary the solution of equations (6) to (8) for a transitional boundary layer differs from that for the turbulent boundary layer only in that the following auxiliary relations are used; local-wall friction coefficient (eq. (C2)), boundary-layer velocity profile (eq. (12) and eq. (C3)), and boundary-layer temperature-velocity profile (eq. (C5)). As was the case for a turbulent boundary layer, three integral differential equations are generated with three unknowns; A_2, C, and the boundary-layer thickness change.

REFERENCES

1. Eggers, A. J., Jr.; Petersen, R. H.; and Cohen, N. B.: Hypersonic Aircraft Technology and Applications. Astronaut. Aeronaut., vol. 8, no. 6, June 1970, pp. 31-41.

2. Gregory, Thomas J.; Williams, Louis J.; and Wilcox, Darrell E.: The Airbreathing Launch Vehicle for Earth Orbit Shuttle – Performance and Operation. AIAA Paper No. 70-270, Feb. 1970.

3. Henry, John R.; and McLellan, Charles H.: The Air-Breathing Launch Vehicle for Earth-Orbit Shuttle – New Technology and Development Approach. AIAA Paper No. 70-269, Feb. 1970.

4. Bertram, Mitchel H., moderator: Panel and General Discussion. Compressible Turbulent Boundary Layers, NASA SP-216, 1969, pp. 547-564.

5. Beckwith, Ivan E.: Recent Advances In Research on Compressible Turbulent Boundary Layers. Analytic Methods in Aircraft Aerodynamics, NASA SP-228, 1970, pp. 355-416.

6. Harris, Julius E.: Numerical Solution of the Equations for Compressible Laminar, Transitional, and Turbulent Boundary Layers and Comparisons With Experimental Data. NASA TR R-368, 1971.

7. Herring, H. James; and Mellor, George L.: A Method of Calculating Compressible Turbulent Boundary Layers. NASA CR-1144, 1968.

8. Fish, R. W.; and McDonald, H.: Practical Calculations of Transitional Boundary Layers. Rep. UAR-H48, United Aircraft Corp., Mar. 14, 1969.

9. Bushnell, Dennis M.; and Beckwith, Ivan E.: Calculation of Nonequilibrium Hypersonic Turbulent Boundary Layers and Comparisons With Experimental Data. AIAA J., vol. 8, no. 8, Aug. 1970, pp. 1462-1469.

10. Lynes, Larry L.; Nielsen, Jack N.; and Goodwin, Frederick K.: Inhibition of Flow Separation at High Speed. AFFDL-TR-68-119, Vols. I-IV, U.S. Air Force, Mar. 1969.

11. Lynes, Larry L.; Nielsen, Jack N.; and Kuhn, Gary D.: Calculation of Compressible Turbulent Boundary Layers With Pressure Gradients and Heat Transfer. NASA CR-1303, 1969.

12. Alber, Irwin E.; and Coats, Douglas E.: Analytical Investigations of Equilibrium and Nonequilibrium Compressible Turbulent Boundary Layers. AIAA Paper No. 69-689, June 1969.

13. Maslowe, S. A.; and Benson, J. L.: Computer Program for the Design and Analysis of Hypersonic Inlets. Rep. No. 18079 (Contract NAS 2-1460), Lockheed-California Co., Aug. 10, 1964. (Available as NASA CR-77749.)

14. Maslowe, S. A., and Benson, J. L.: A Procedure for Computing Transitional Boundary Layer Parameters in Compressible Flows. Rep. No. LR 20405, Lockheed-California Co., Jan. 4, 1967.

15. Kutschenreuter, Paul H., Jr.; Keith, James S.; Weil, James A.; and Nettleton, Paul H.: Investigation of Hypersonic Inlet Shock-Wave Boundary Layer Interaction. AFFDL-TR-65-36, U.S. Air Force, Mar. 1965. (Available from DDC as AD 464 057.)

16. Reshotko, Eli; and Tucker, Maurice: Approximate Calculation of the Compressible Turbulent Boundary Layer With Heat Transfer and Arbitrary Pressure Gradient. NACA TN 4154, 1957.

17. Henry, J. R.; Andrews, E. H., Jr.; Pinckney, S. Z.; and McClinton, C. R.: Boundary Layer and Starting Problems on a Short Axisymmetric Scramjet Inlet. Compressible Turbulent Boundary Layers, NASA SP-216, 1968, pp. 481-508.

18. Pinckney, S. Z.: Static-Temperature Distribution in a Flat-Plate Compressible Turbulent Boundary Layer With Heat Transfer. NASA TN D-4611, 1968.

19. Schlichting, Hermann (J. Kestin, transl.): Boundary Layer Theory. McGraw-Hill Book Co., Inc., 1955.

20. Neal, Luther, Jr.; and Bertram, Mitchel H.: Turbulent-Skin-Friction and Heat-Transfer Charts Adapted From the Spalding and Chi Method. NASA TN D-3969, 1967.

21. Bertram, Mitchel H.; and Neal, Luther, Jr.: Recent Experiments in Hypersonic Turbulent Boundary Layers. Presented at the AGARD Specialists Meeting on Recent Developments in Boundary-Layer Research (Naples, Italy), May 1965.

22. Maise, George; and McDonald, Henry: Mixing Length and Kinematic Eddy Viscosity in a Compressible Boundary Layer. AIAA J., vol. 6, no. 1, Jan. 1968, pp. 73-80.

23. Coles, Donald: The Law of the Wake in the Turbulent Boundary Layer. J. Fluid Mech., vol. 1, pt. 2, July 1956, pp. 191-226.

24. Bradshaw, P.: The Response of a Constant-Pressure Turbulent Boundary Layer to the Sudden Application of an Adverse Pressure Gradient. NPL Aero Rep. 1219, Brit. A.R.C., Jan. 6, 1967.

25. Cubbage, James M.: Effect of Nose Bluntness and Controlled Roughness on the Flow on Two Hypersonic Inlet Center Bodies Without Cowling at Mach 5.98. NASA TN D-2900, 1965.

26. Stroud, J. F.; and Miller, L. D.: An Experimental and Analytical Investigation of Hypersonic Inlet Boundary Layers. Vol. II. Data Reduction Program and Tabulated Experimental Data. AFFDL-TR-65-123-Vol. II, U.S. Air Force, Aug. 1965. (Available from DDC as AD 621 344.)

27. Wilson, R. E.: Characteristics of Turbulent Boundary Layer Flow Over a Smooth, Thermally Insulated Flat Plate at Supersonic Speeds. DRL-301, CM-712 (Contract NOrd-9195), Univ. of Texas, June 1, 1952.

28. Kepler, C. E.; and O'Brien, R. L.: Supersonic Turbulent Boundary Layer Growth Over Cooled Walls in Adverse Pressure Gradients. ASD-TDR-62-87, U.S. Air Force, Oct. 1962.

29. Danberg, James E.: Characteristics of the Turbulent Boundary Layer With Heat and Mass Transfer at M=6.7. NOLTR 64-99, U.S. Navy, Oct. 19, 1964. (Available from DDC as AD 452 471.)

30. Lomax, Harvard; and Inouye, Mamoru: Numerical Analysis of Flow Properties About Blunt Bodies Moving at Supersonic Speeds in an Equilibrium Gas. NASA TR R-204, 1964.

31. Inouye, Mamoru: Blunt Body Solutions for Spheres and Ellipsoids in Equilibrium Gas Mixtures. NASA TN D-2780, 1965.

32. Inouye, Mamoru; Rakich, John V.; and Lomax, Harvard: A Description of Numerical Methods and Computer Programs for Two-Dimensional and Axisymmetric Supersonic Flow Over Blunt-Nosed and Flared Bodies. NASA TN D-2970, 1965.

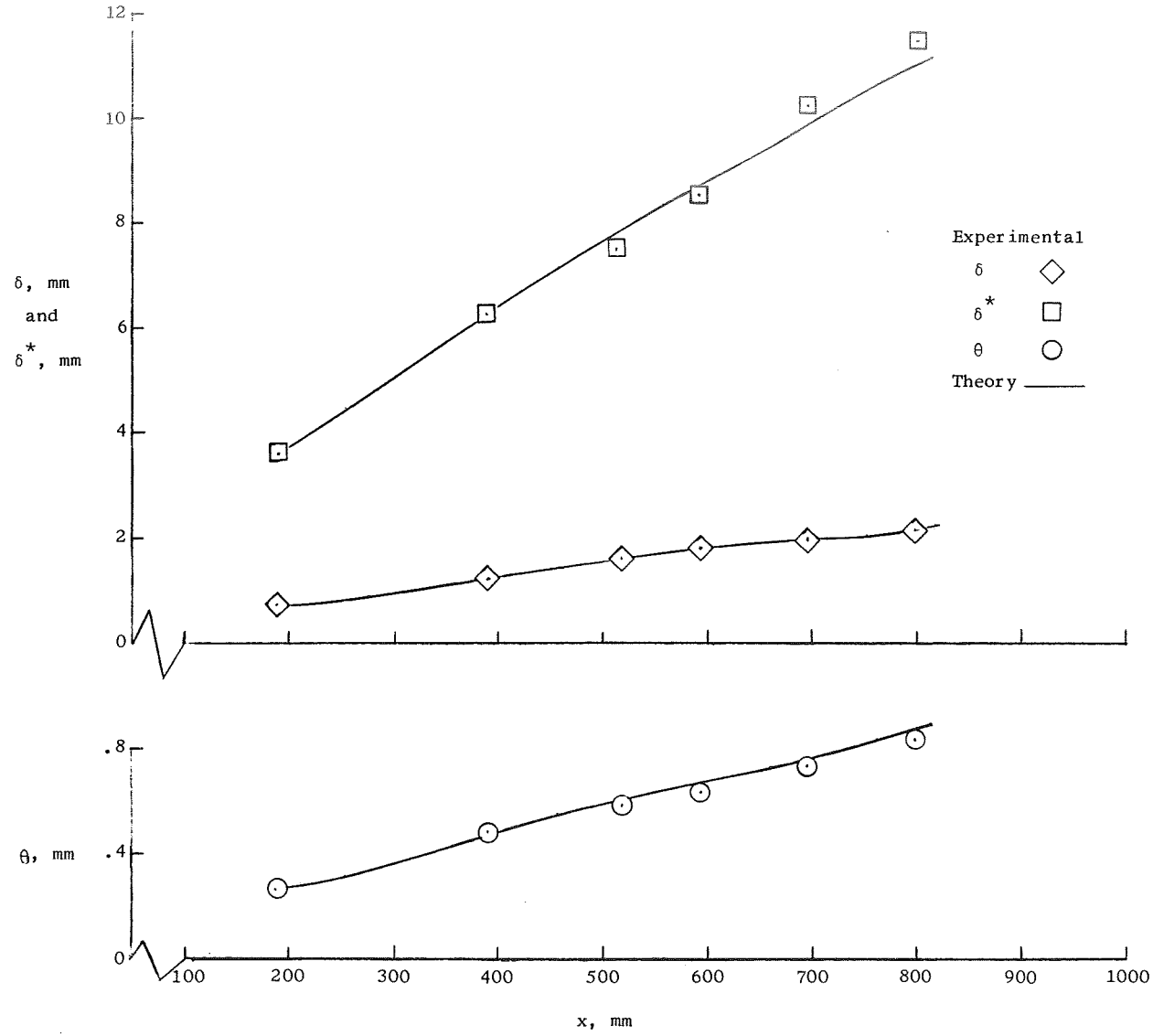

(a) $M_\delta = 1.73$; adiabatic wall.

Figure 1.- Boundary-layer development on flat plate of reference 27.

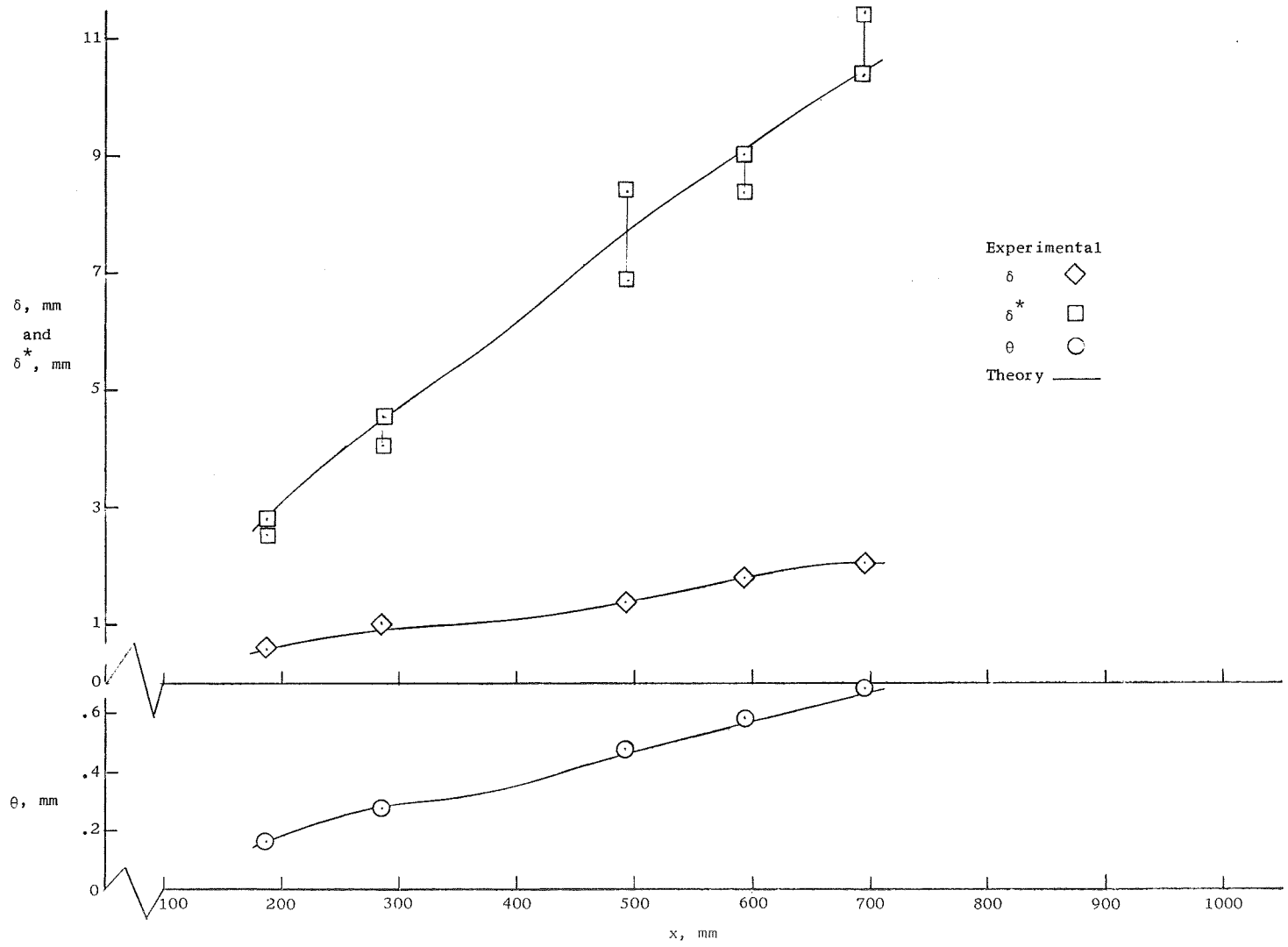

(b) $M_\delta = 2.0$; adiabatic wall.

Figure 1.- Continued.

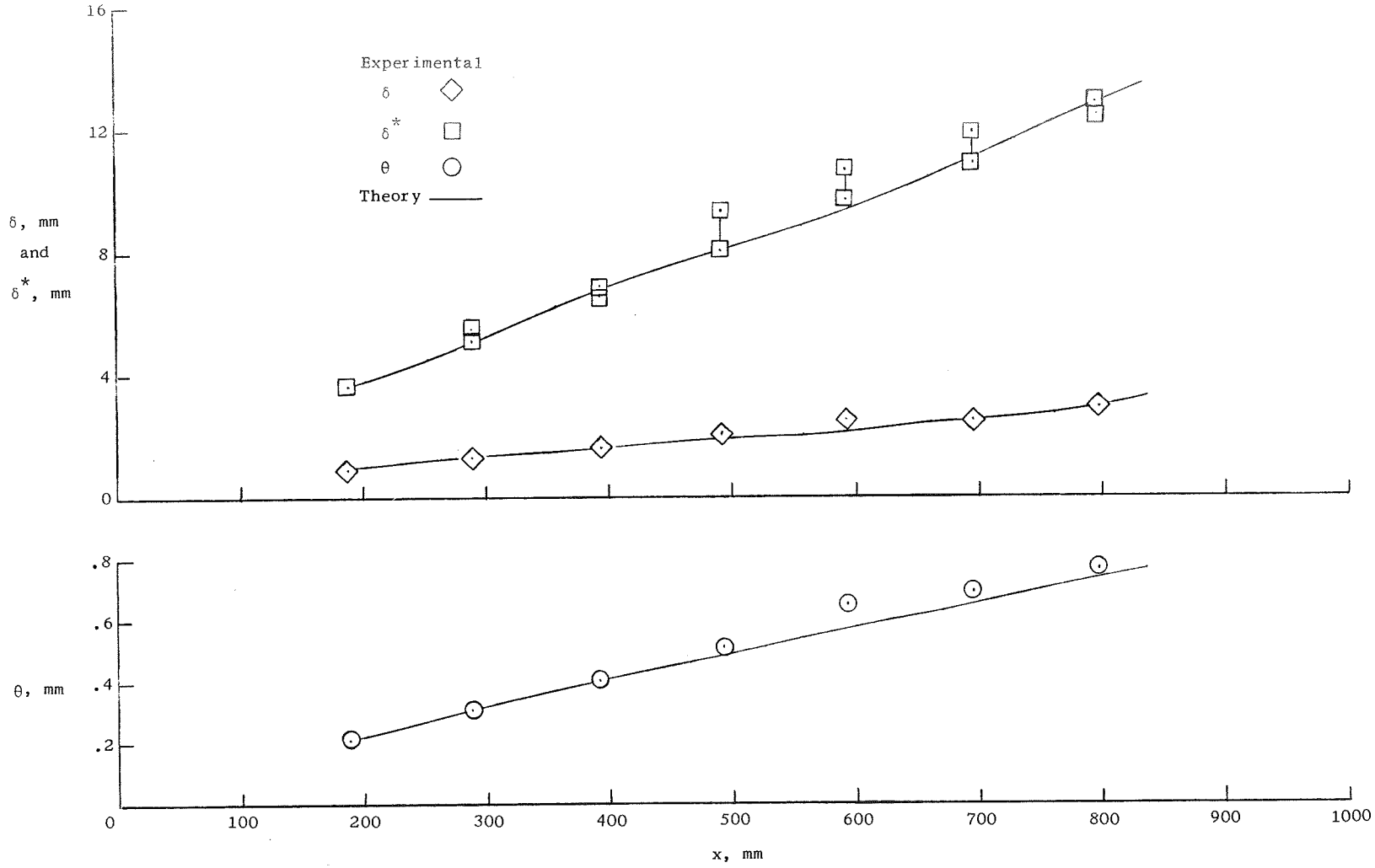

(c) $M_\delta = 2.5$; adiabatic wall.

Figure 1.- Concluded.

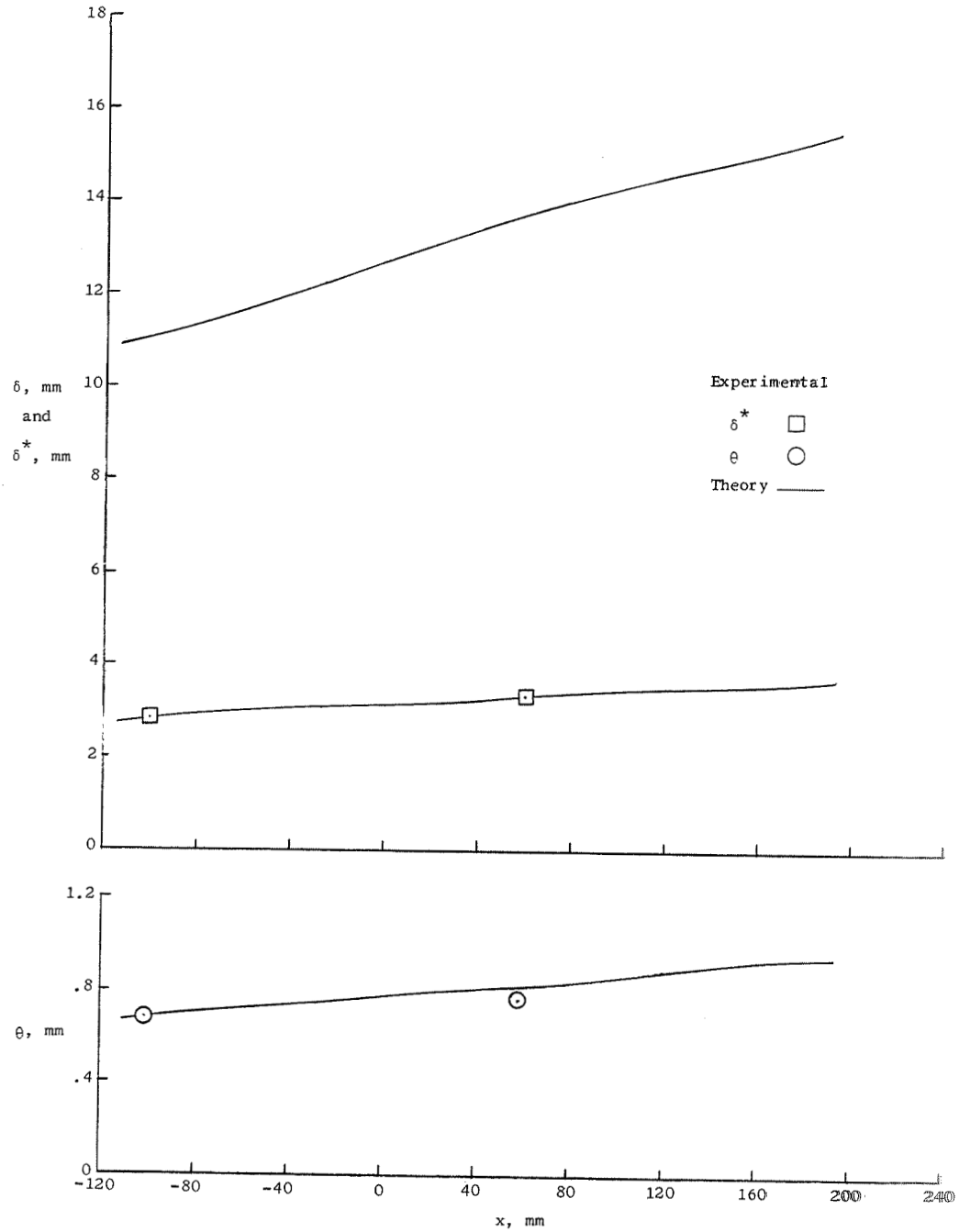

(a) $T_w/T_{t,\delta} = 0.45$.

Figure 2.- Boundary-layer development in constant-pressure region of tunnel wall. Reference 28; $M_\delta = 3.0$.

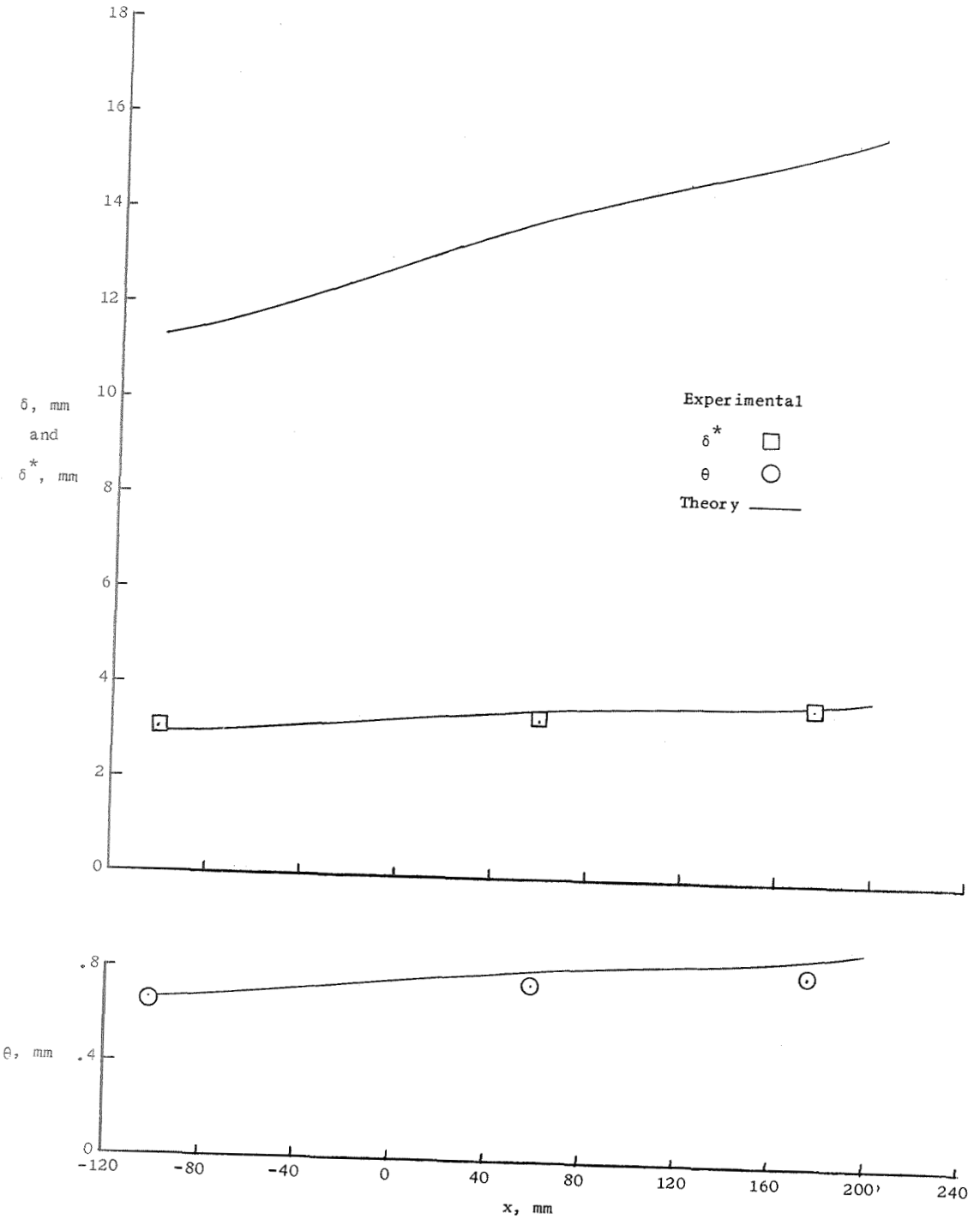

(b) $T_w/T_{t,\delta} = 0.65$.

Figure 2.- Continued.

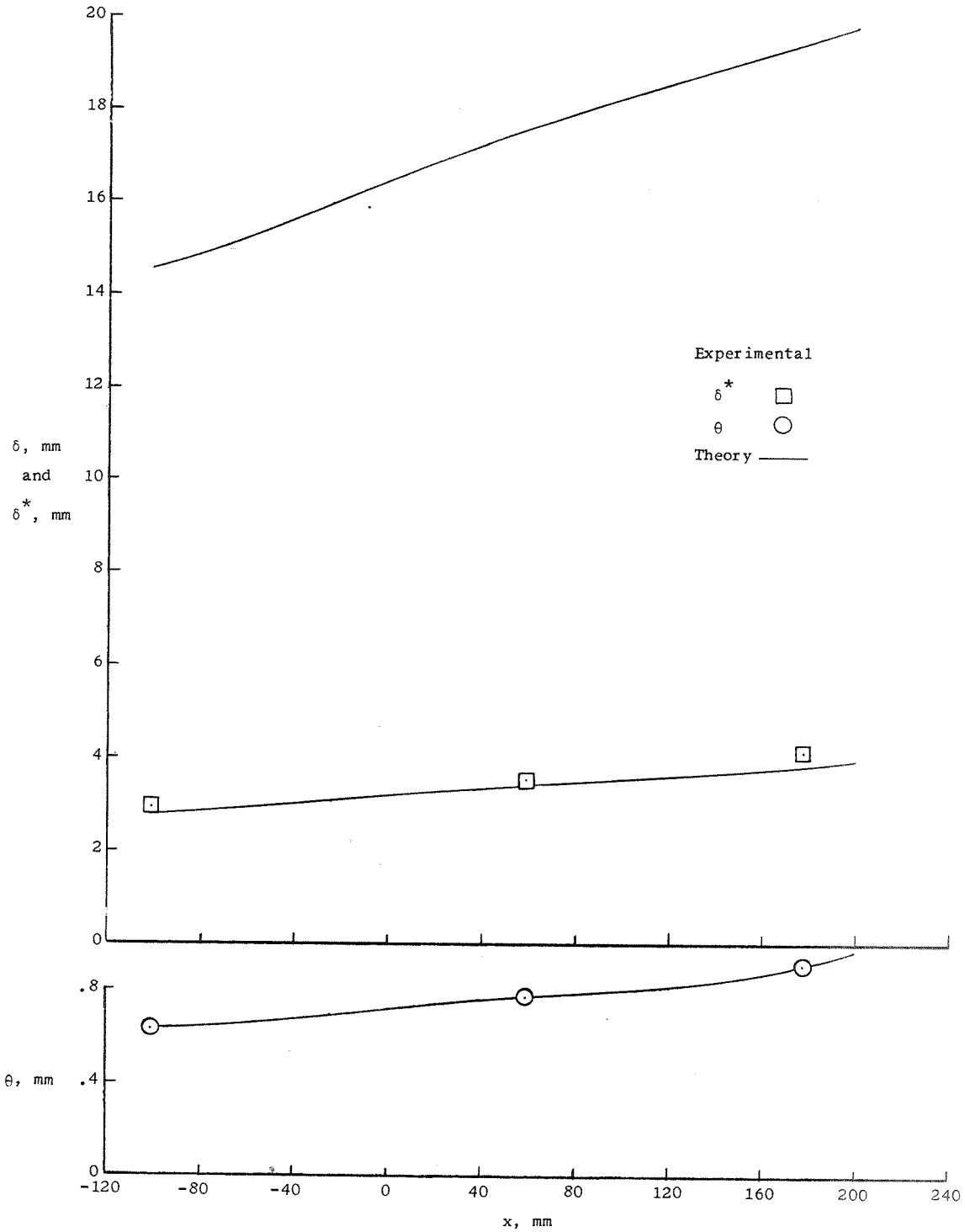

(c) $T_w/T_{t,\delta} = 0.85$.

Figure 2.- Concluded.

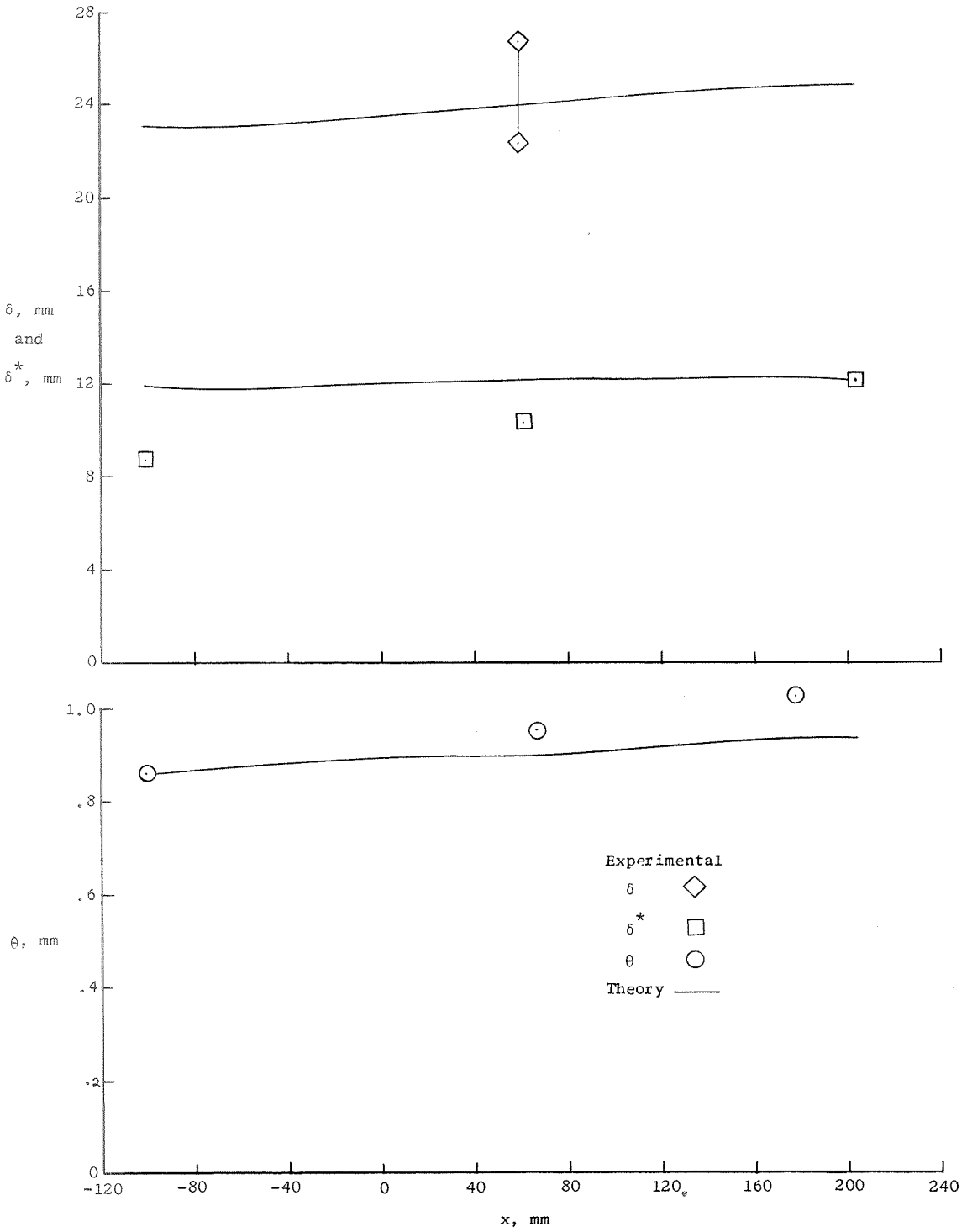

(a) $T_w/T_{t,\delta} = 0.265$.

Figure 3.- Boundary-layer development in constant-pressure region of tunnel wall. Reference 28; $M_\delta = 6.0$.

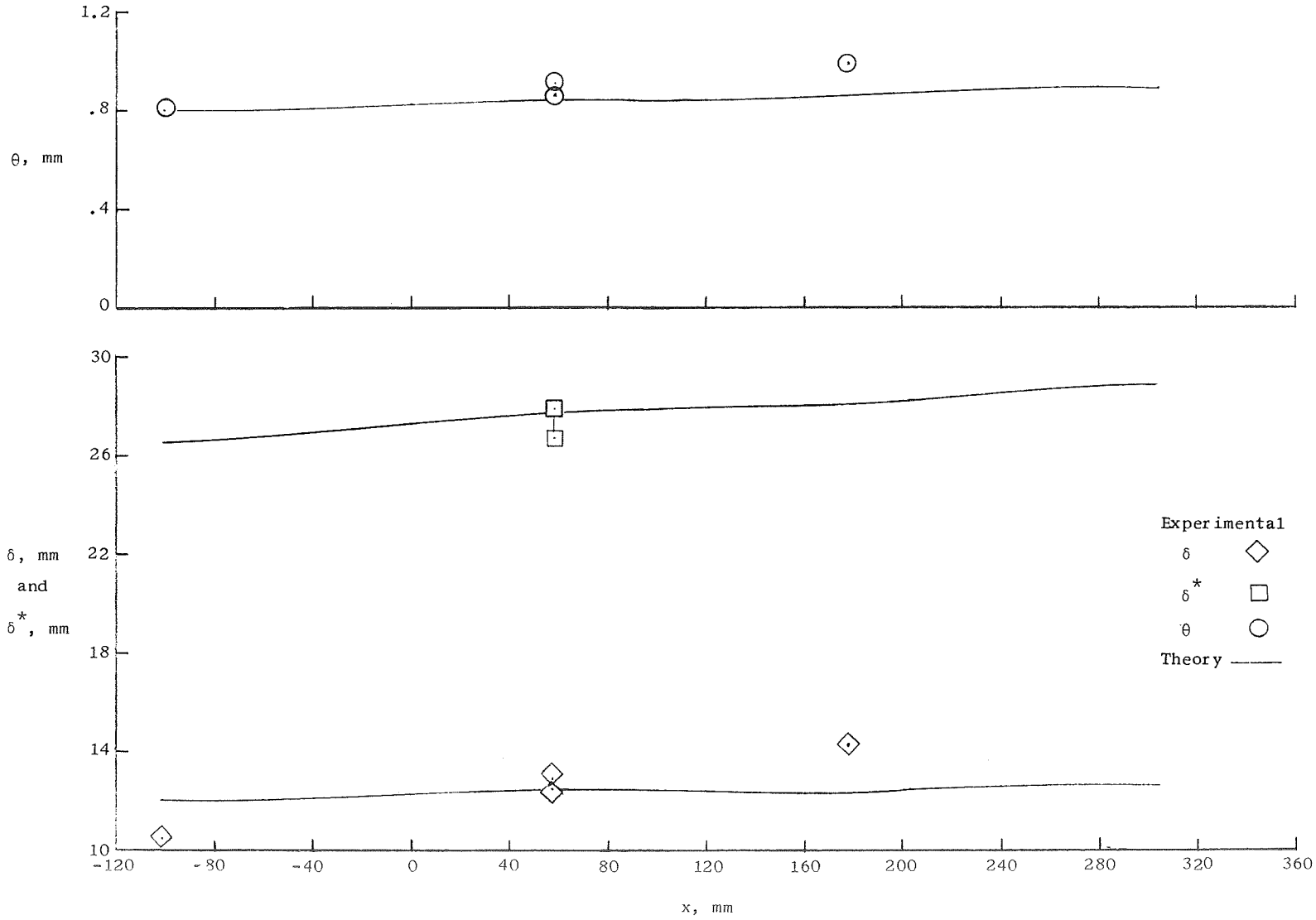

(b) $T_w/T_{t,\delta} = 0.760$.

Figure 3.- Concluded.

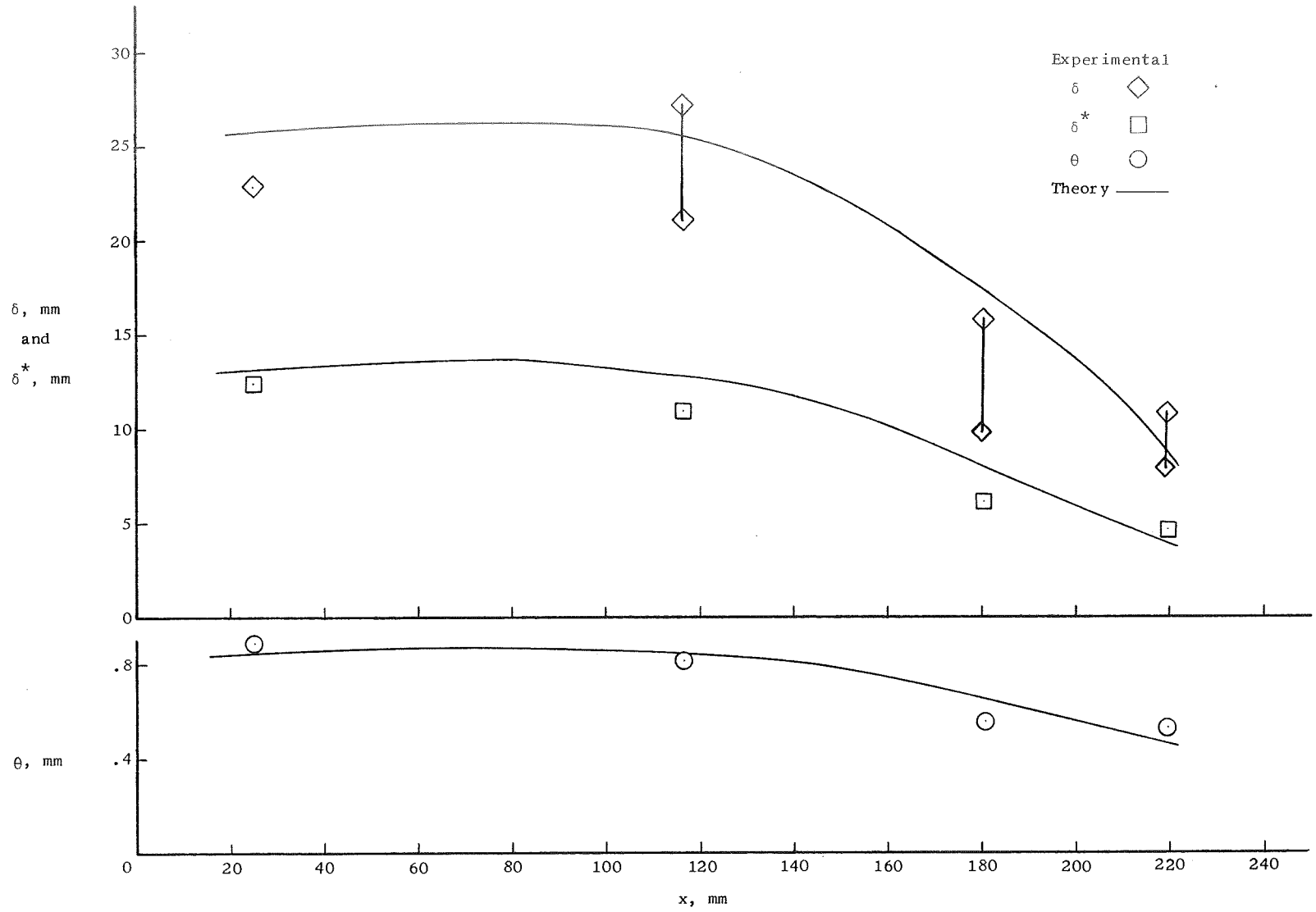

(a) $T_w/T_{t,\delta} = 0.45$.

Figure 4.- Boundary-layer development on two-dimensional compression surface. Reference 28; $M_\delta = 6.0$.

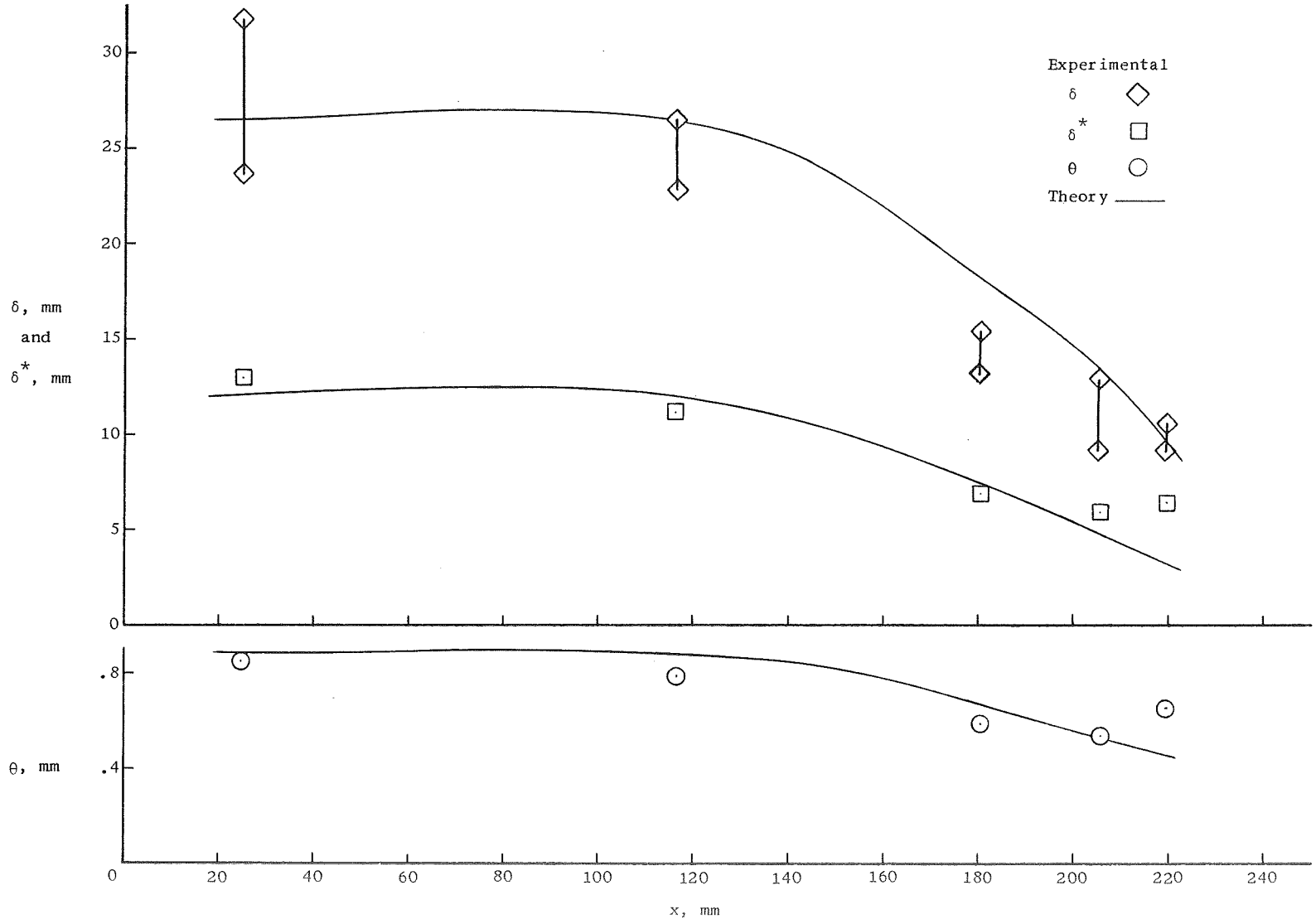

(b) $T_w/T_{t,\delta} = 0.82$.

Figure 4.- Concluded.

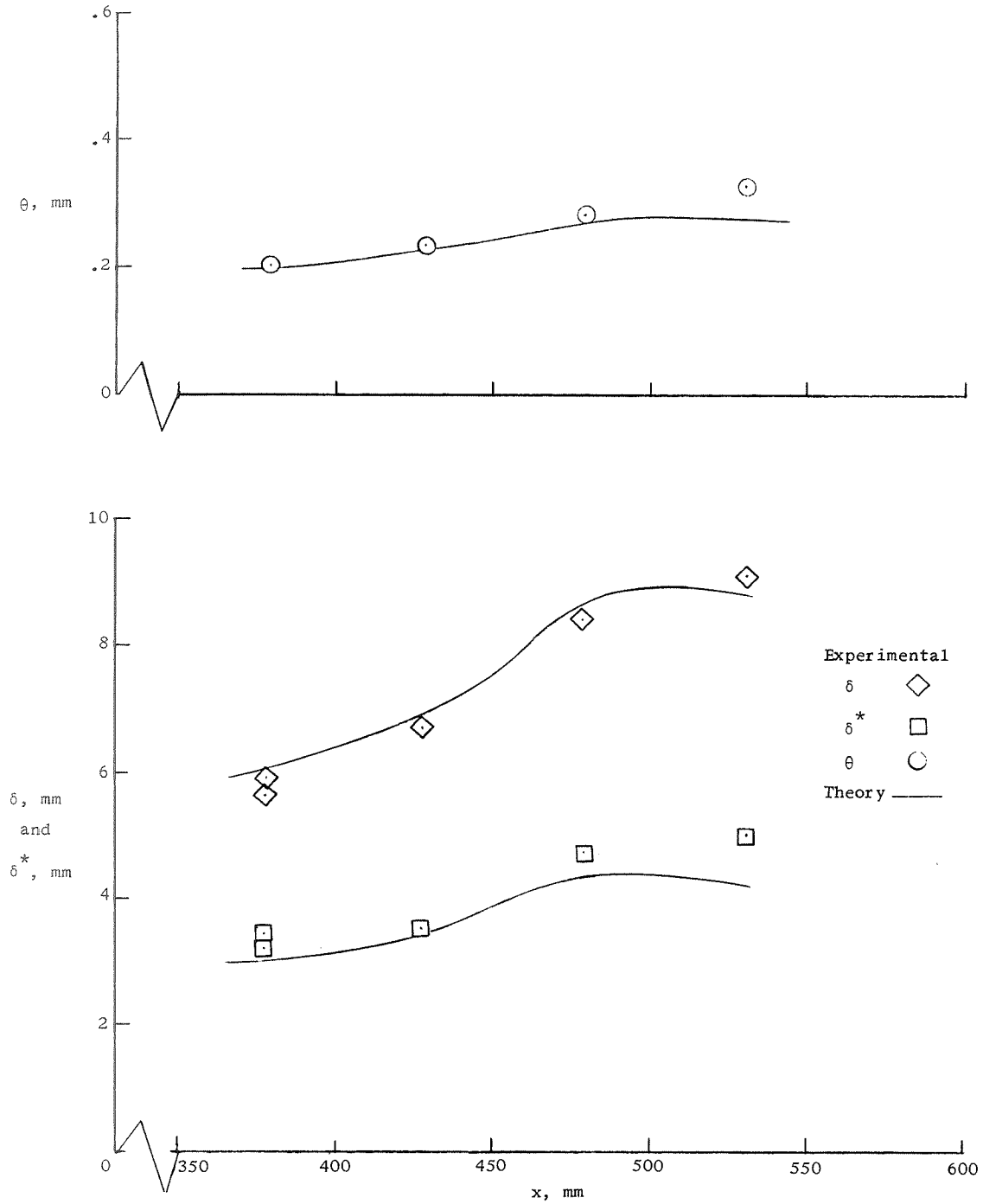

(a) $M_\delta = 6.54$; $T_w/T_{t,\delta} = 0.46$.

Figure 5.- Boundary-layer development on a flat plate. Reference 29.

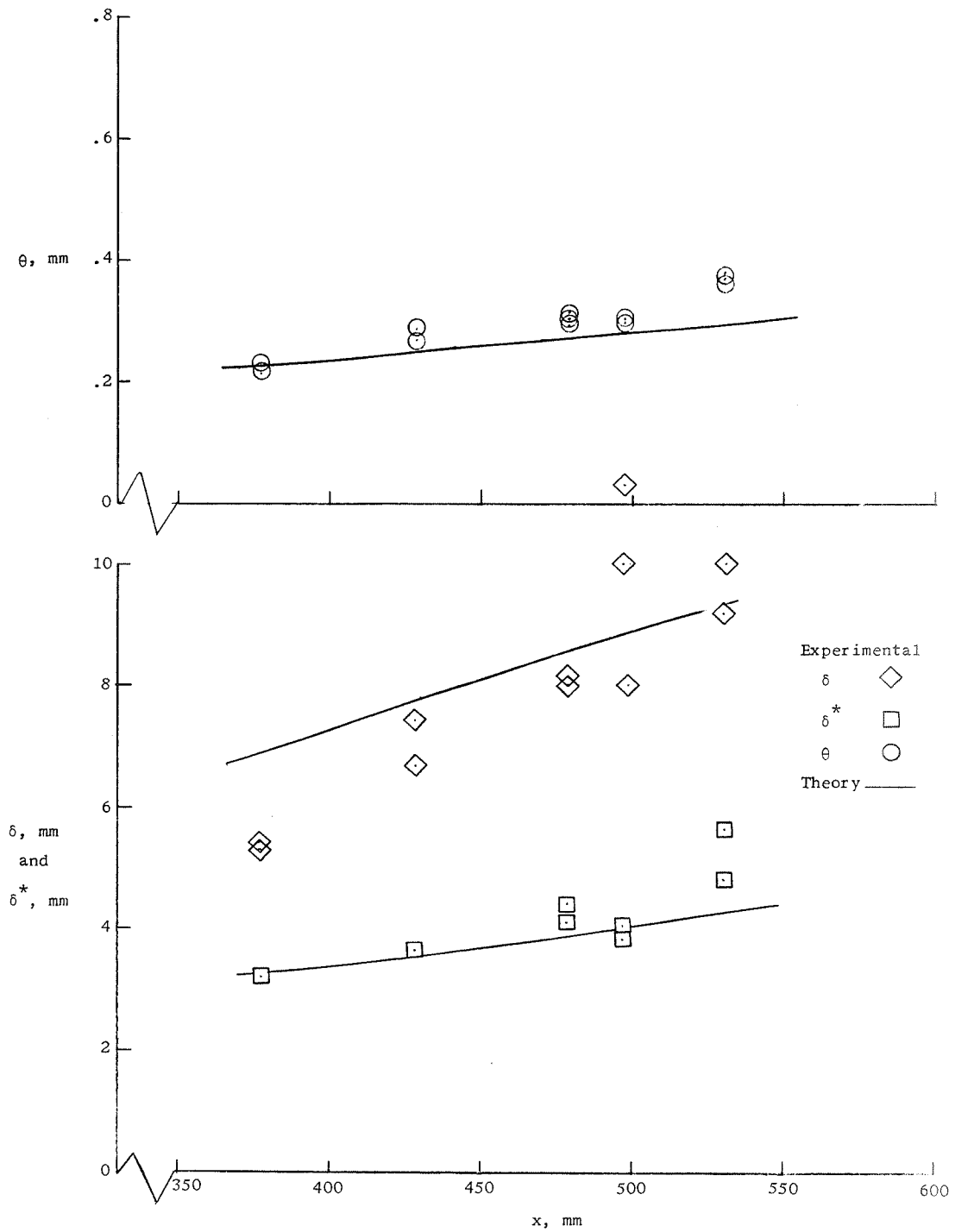

(b) $M_\delta = 6.54$; $T_w/T_{t,\delta} = 0.58$.

Figure 5.- Continued.

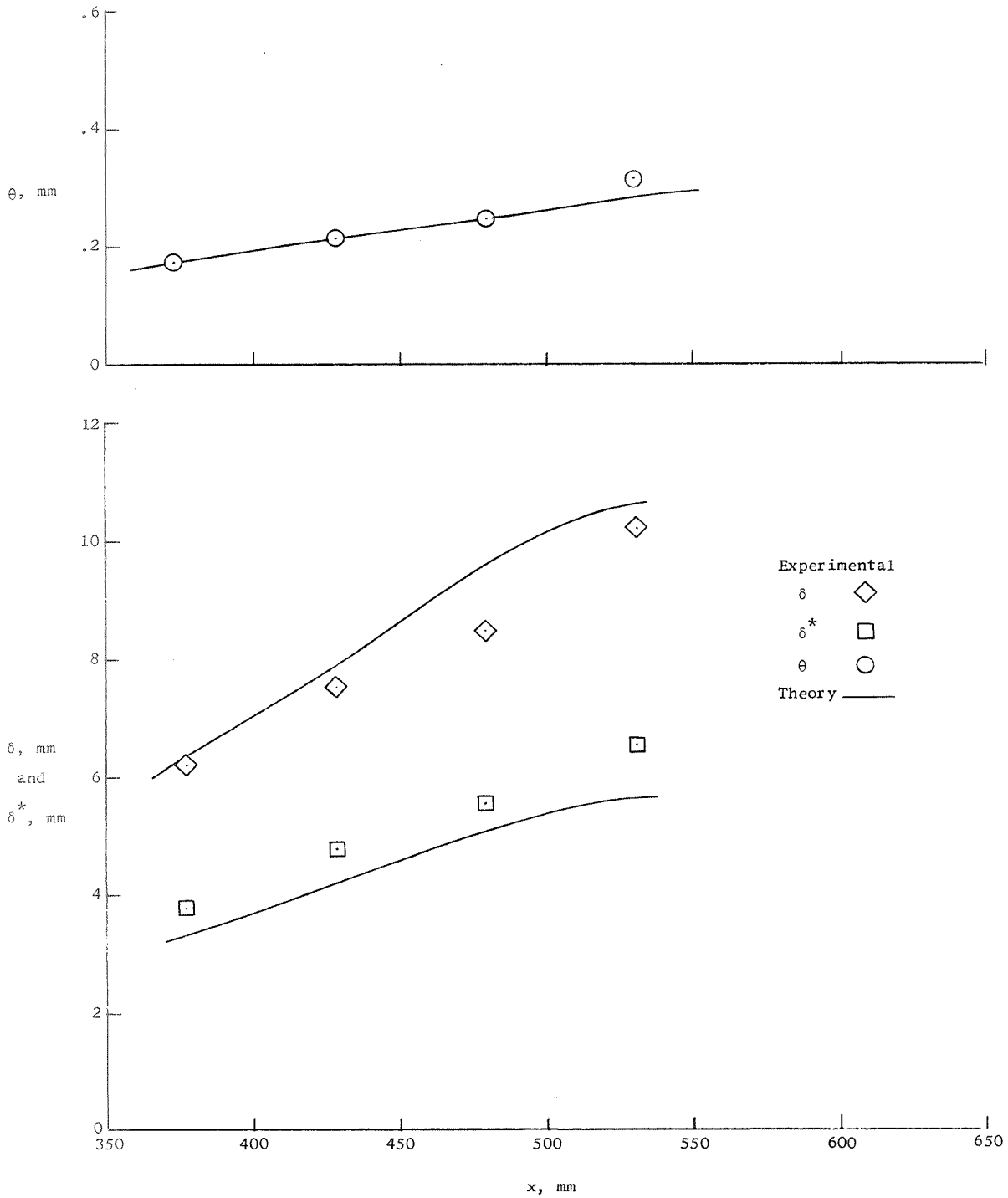

(c) $M_\delta = 6.54$; $T_w/T_{t,\delta} = 0.83$.

Figure 5.- Continued.

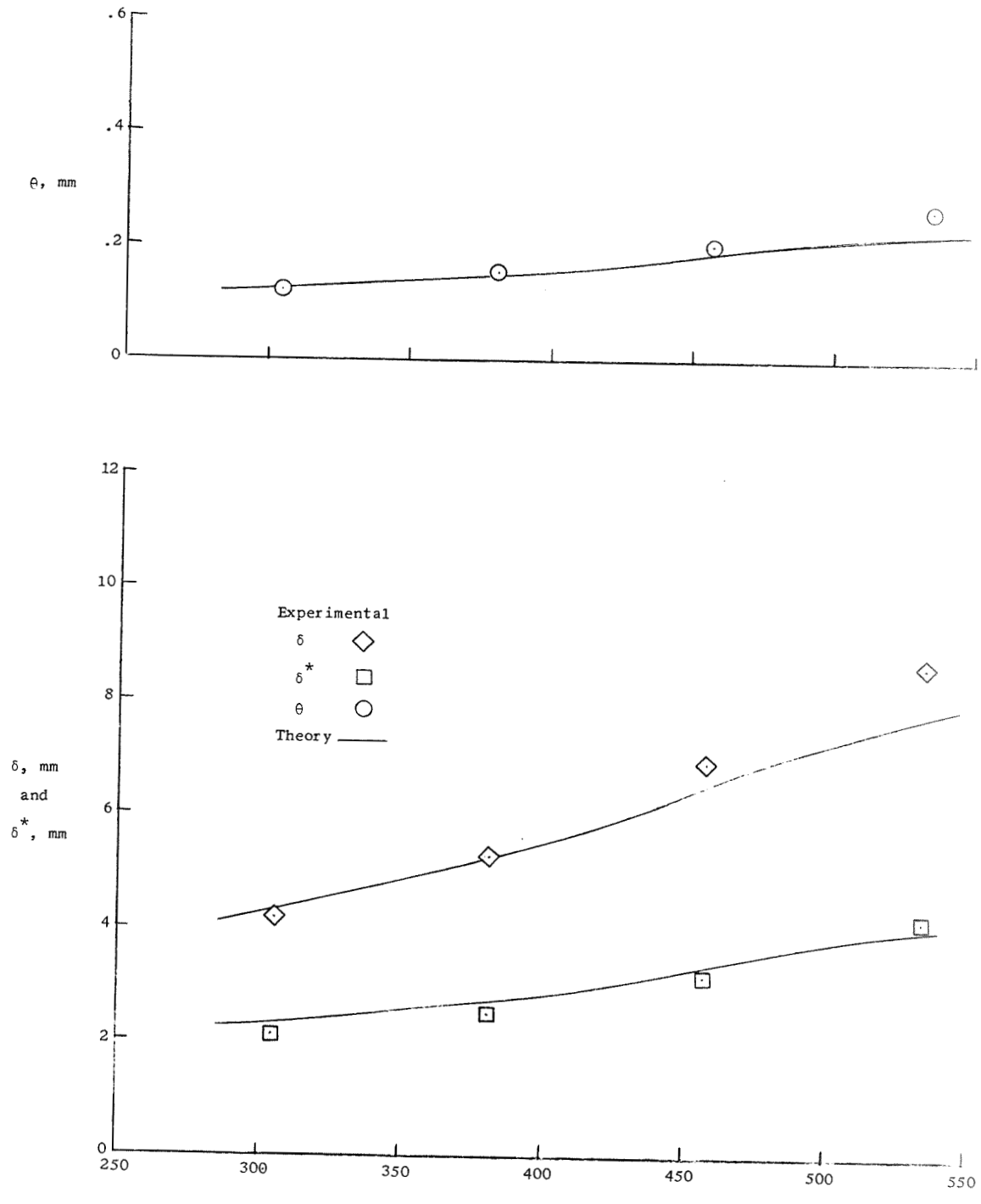

(d) $M_\delta = 6.22$; $T_w/T_{t,\delta} = 0.83$.

Figure 5.- Continued.

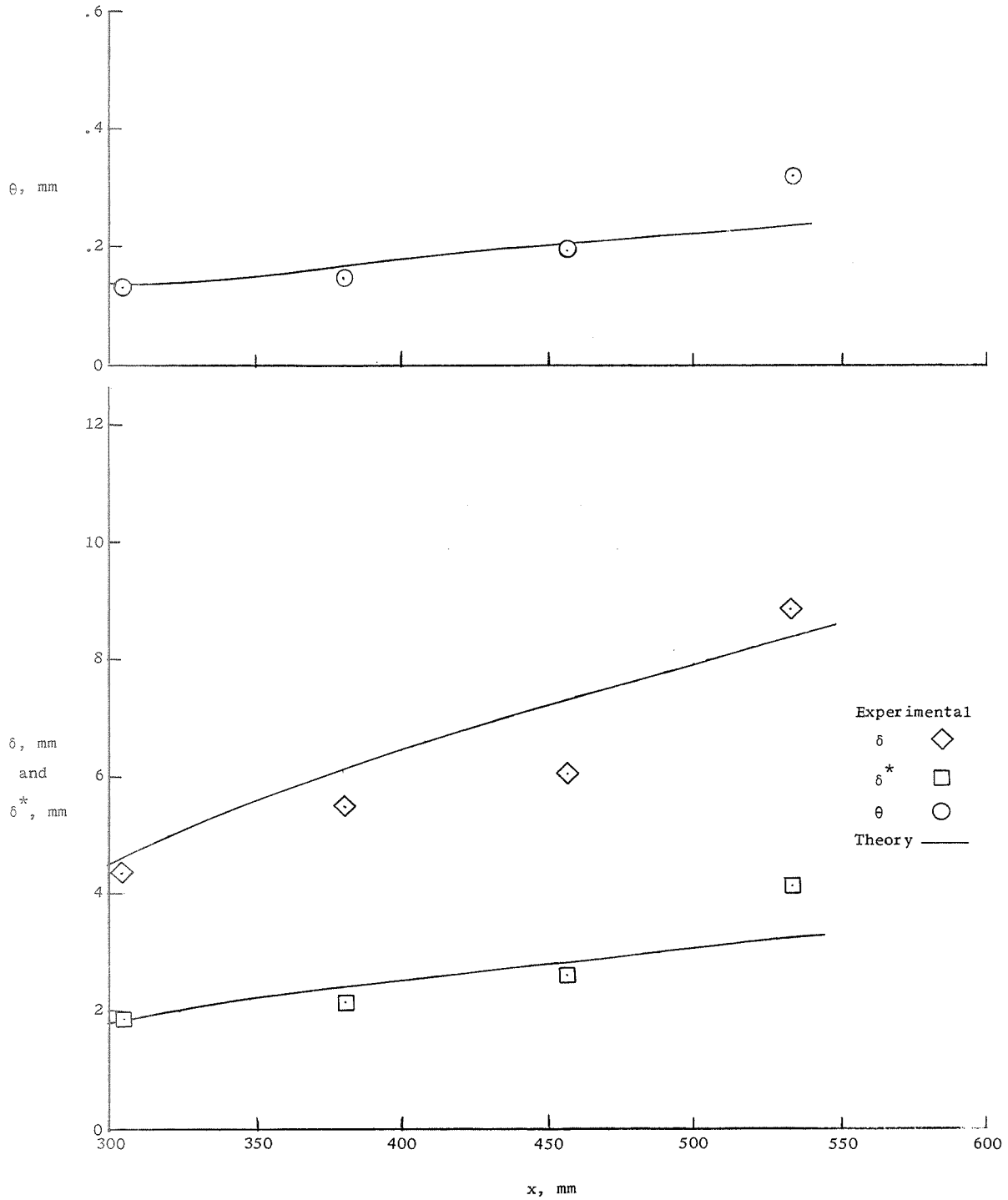

(e) $M_\delta = 6.29$; $T_w/T_{t,\delta} = 0.59$.

Figure 5.- Concluded.

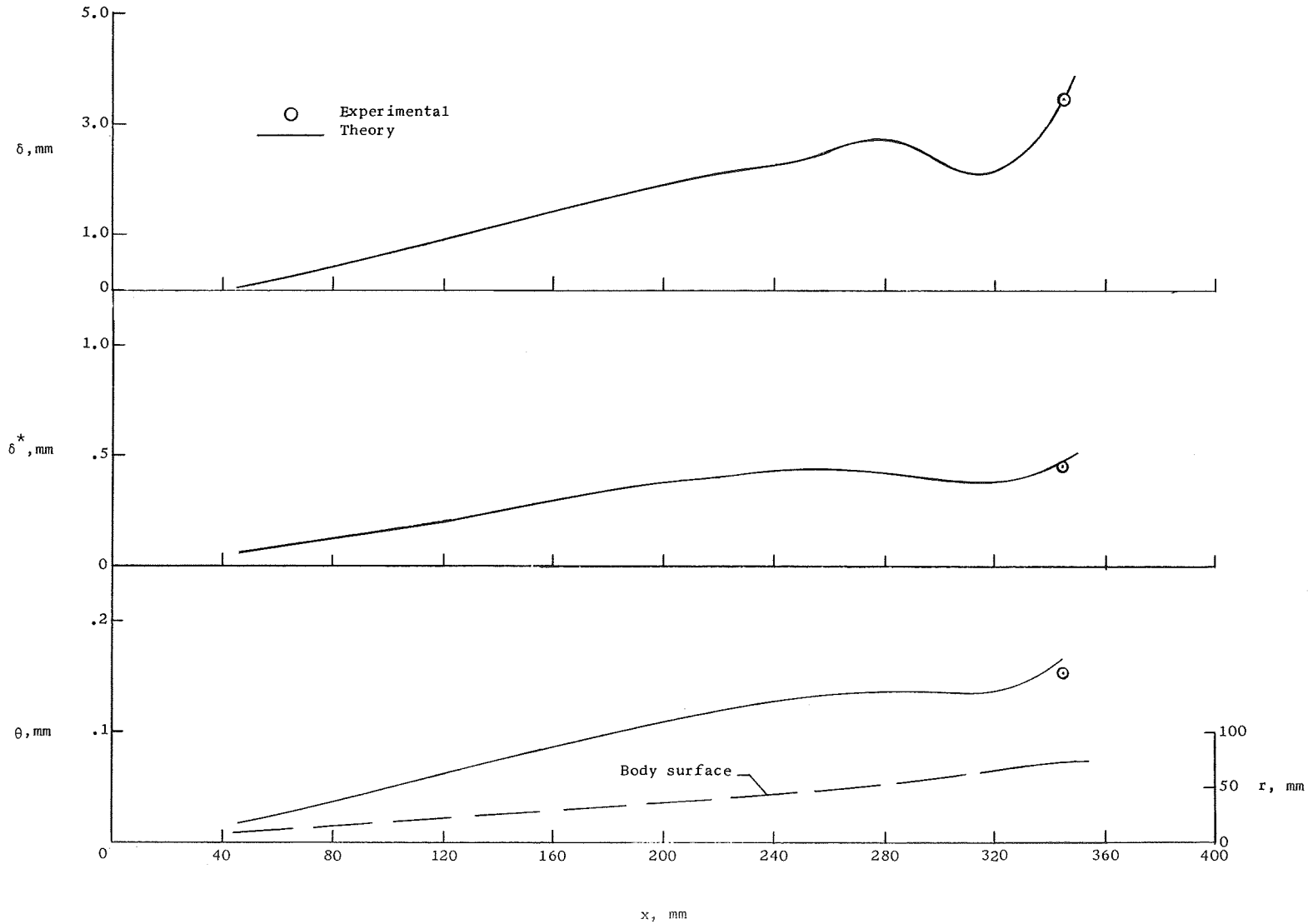

(a) $T_w/T_{t,\delta} = 0.2$.

Figure 6.- Boundary-layer development on axisymmetric body of reference 17. $M_\delta = 4.0$.

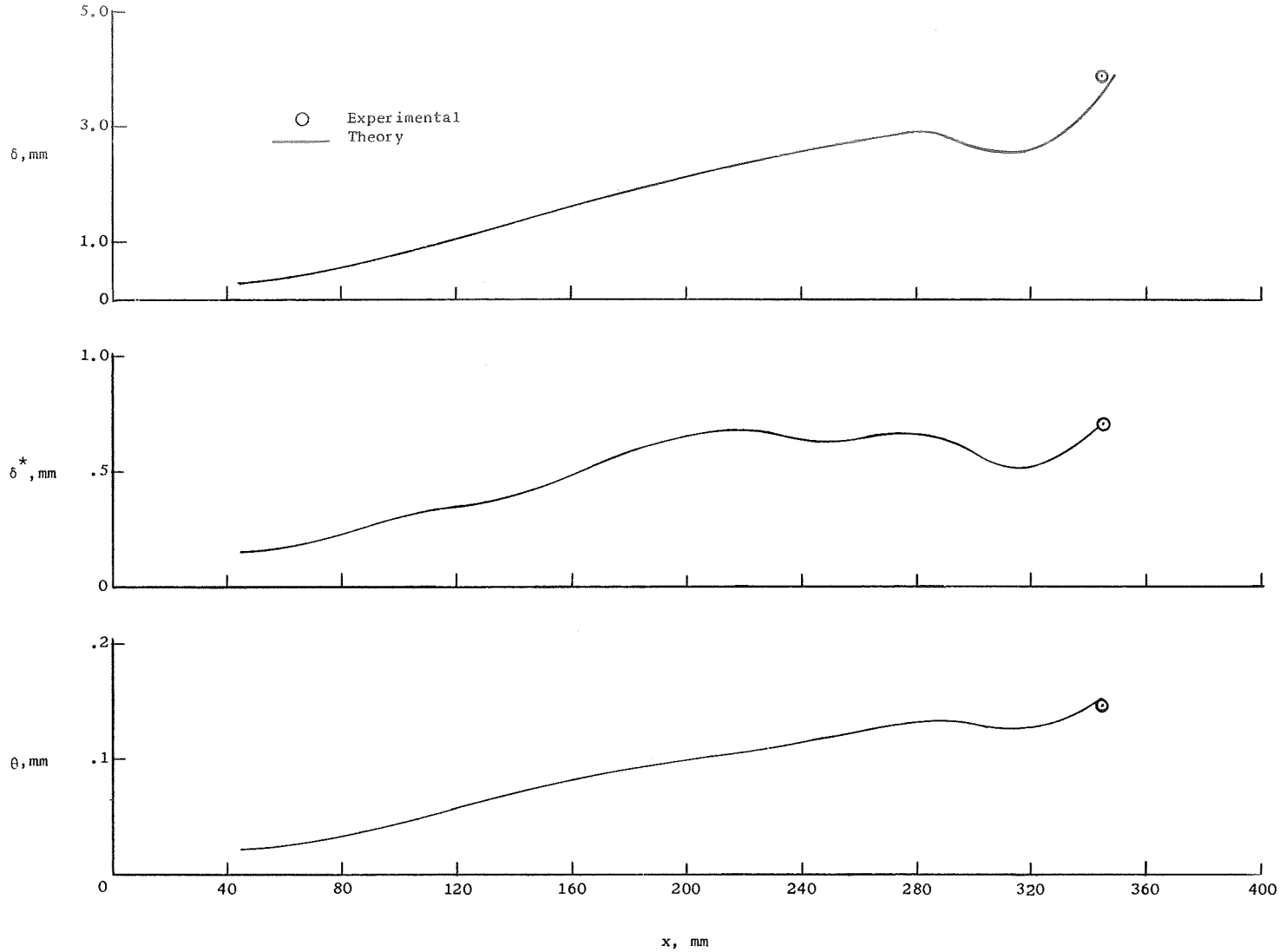

(b) $T_w/T_{t,\delta} = 0.7$.

Figure 6.- Continued.

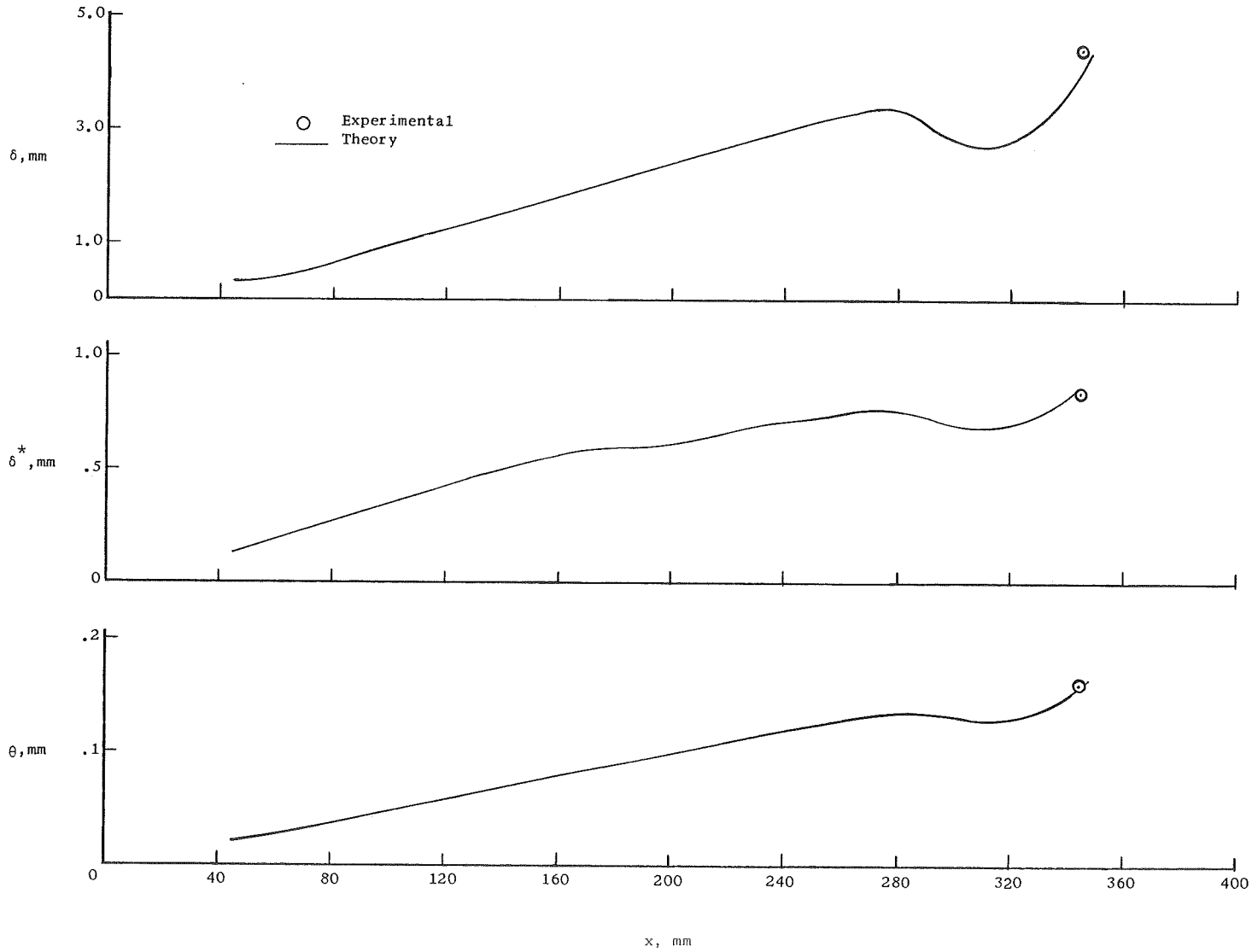

(c) $T_w/T_{t,\delta} = 0.9$.

Figure 6.- Concluded.

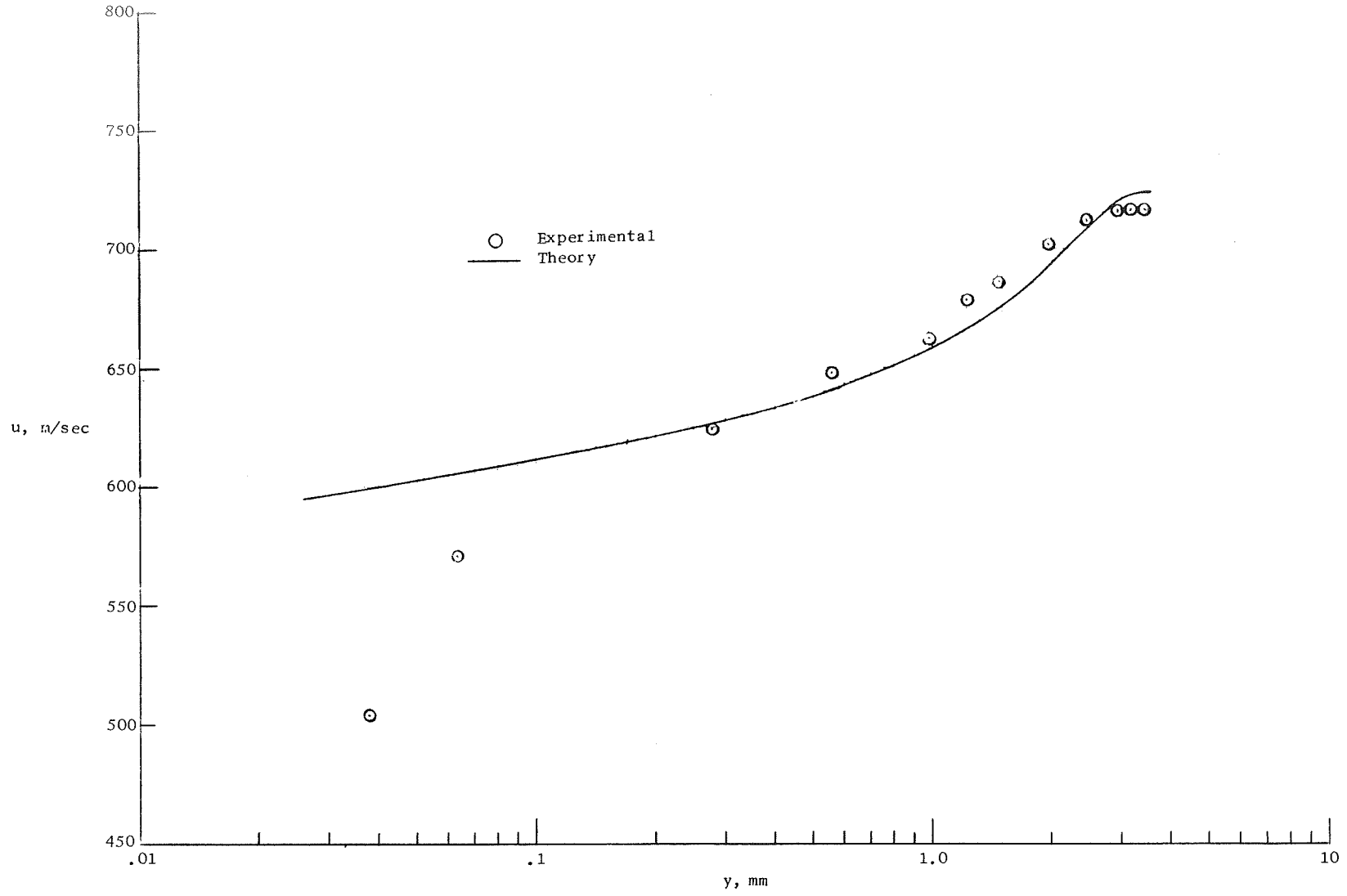

(a) $T_w/T_{t,\delta} = 0.2$.

Figure 7.- Velocity profiles for axisymmetric body of reference 17. $M_\delta = 4.0$; x = 344 mm.

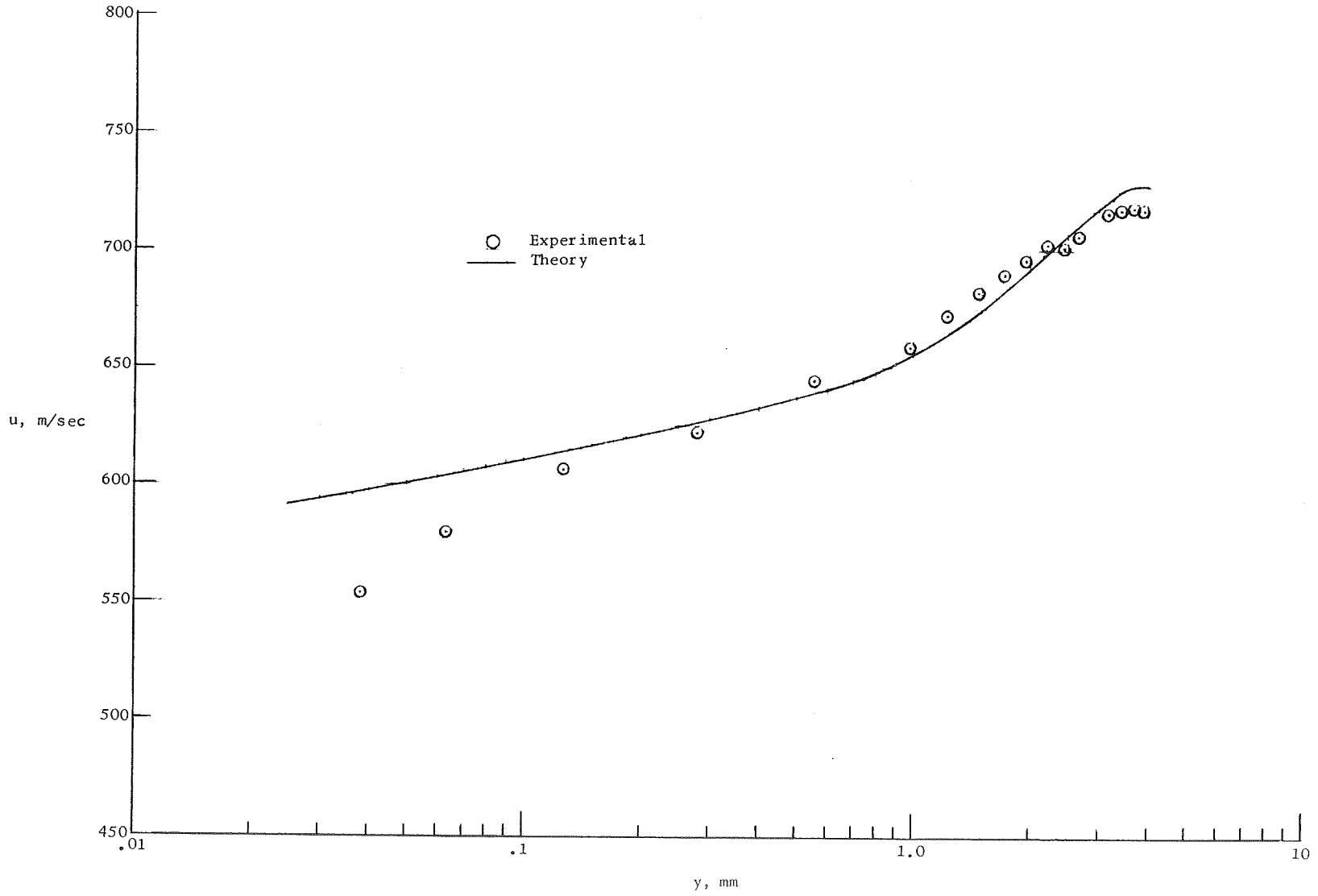

(b) $T_w/T_{t,\delta} = 0.7$.

Figure 7.- Continued.

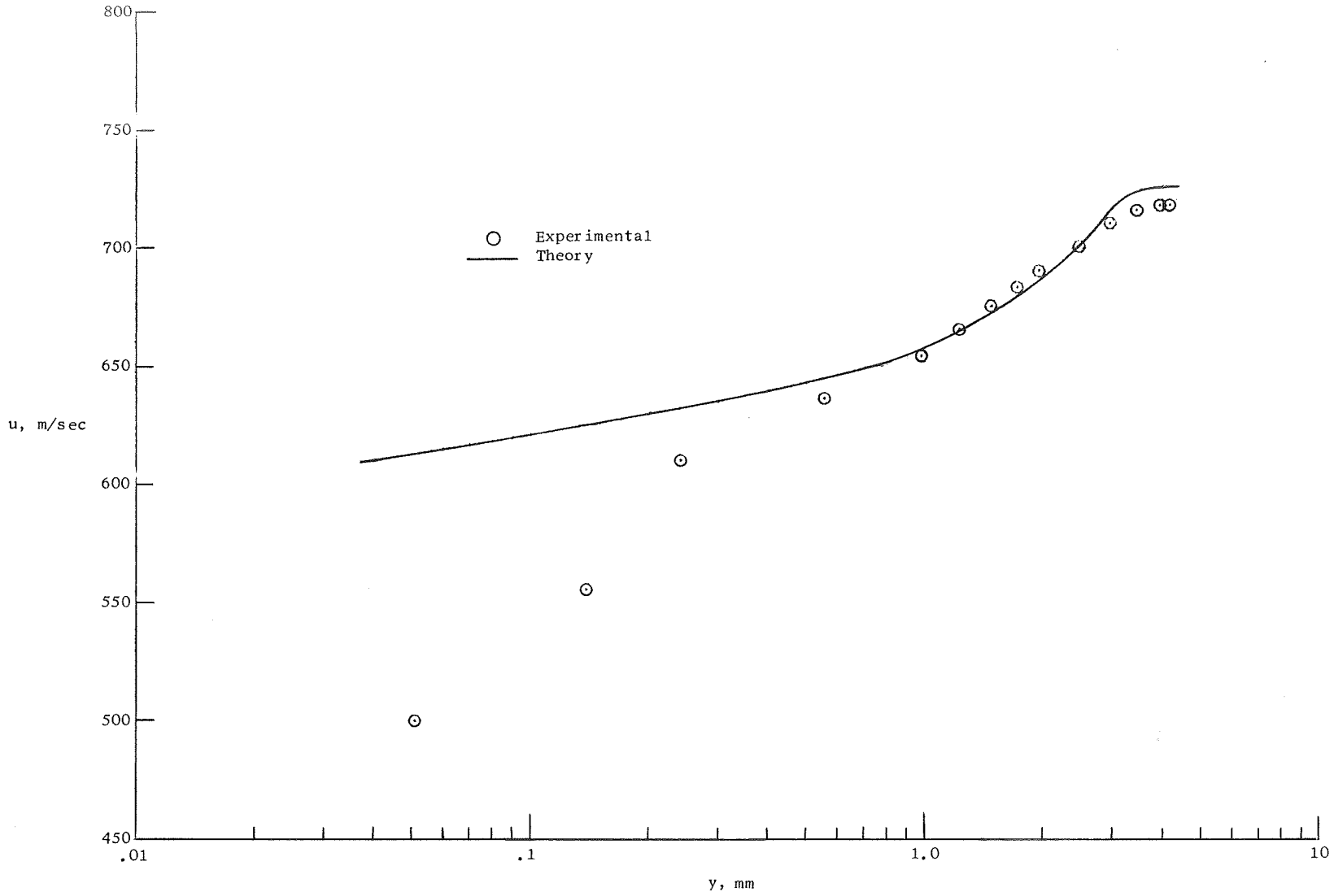

(c) $T_w/T_{t,\delta} = 0.9$.

Figure 7.- Concluded.

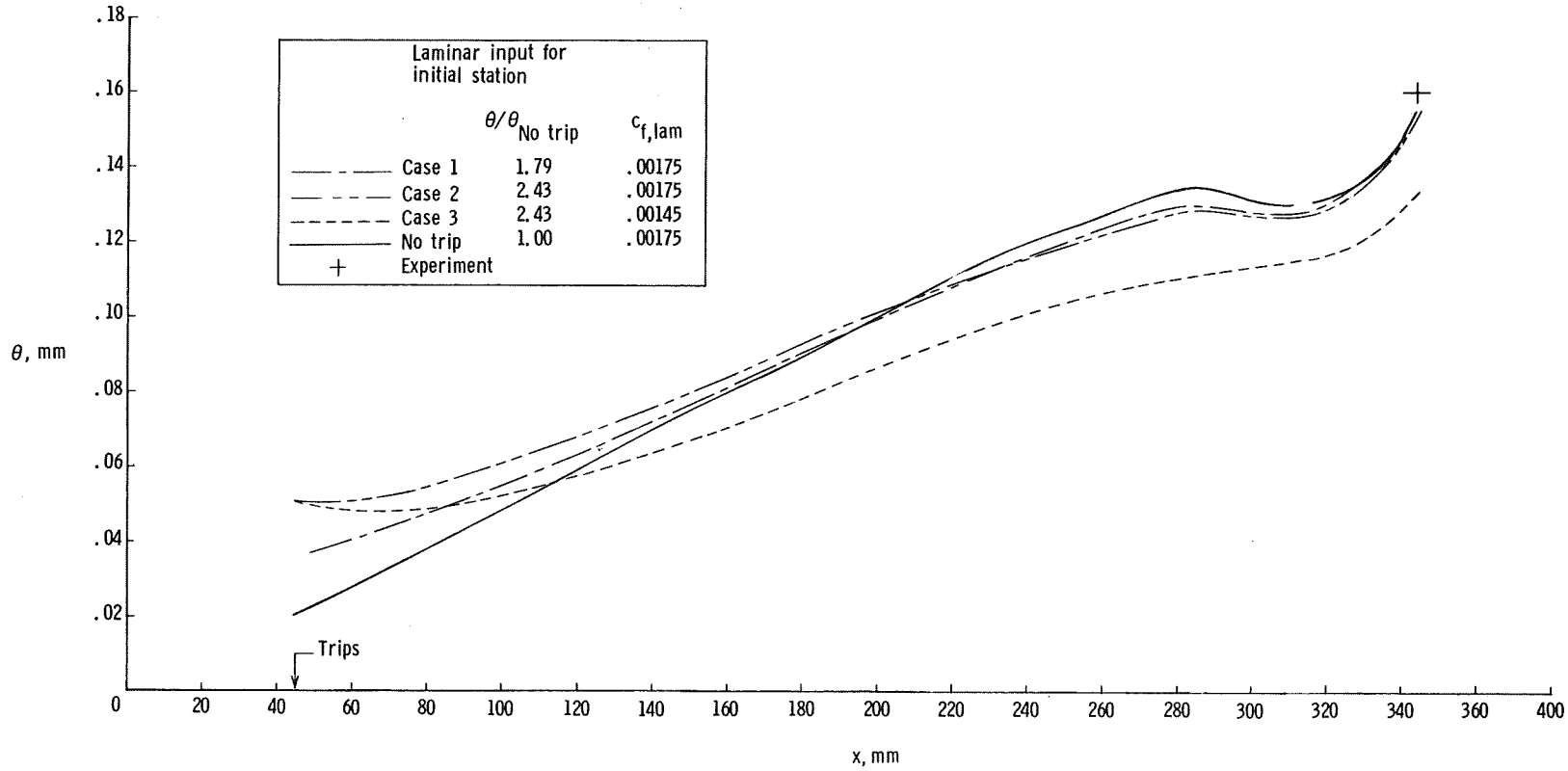

Figure 8.- Effect on theoretical momentum-thickness development of varying initial values of θ and $c_{f,lam}$, data of reference 17. $M_\delta = 4.0$.

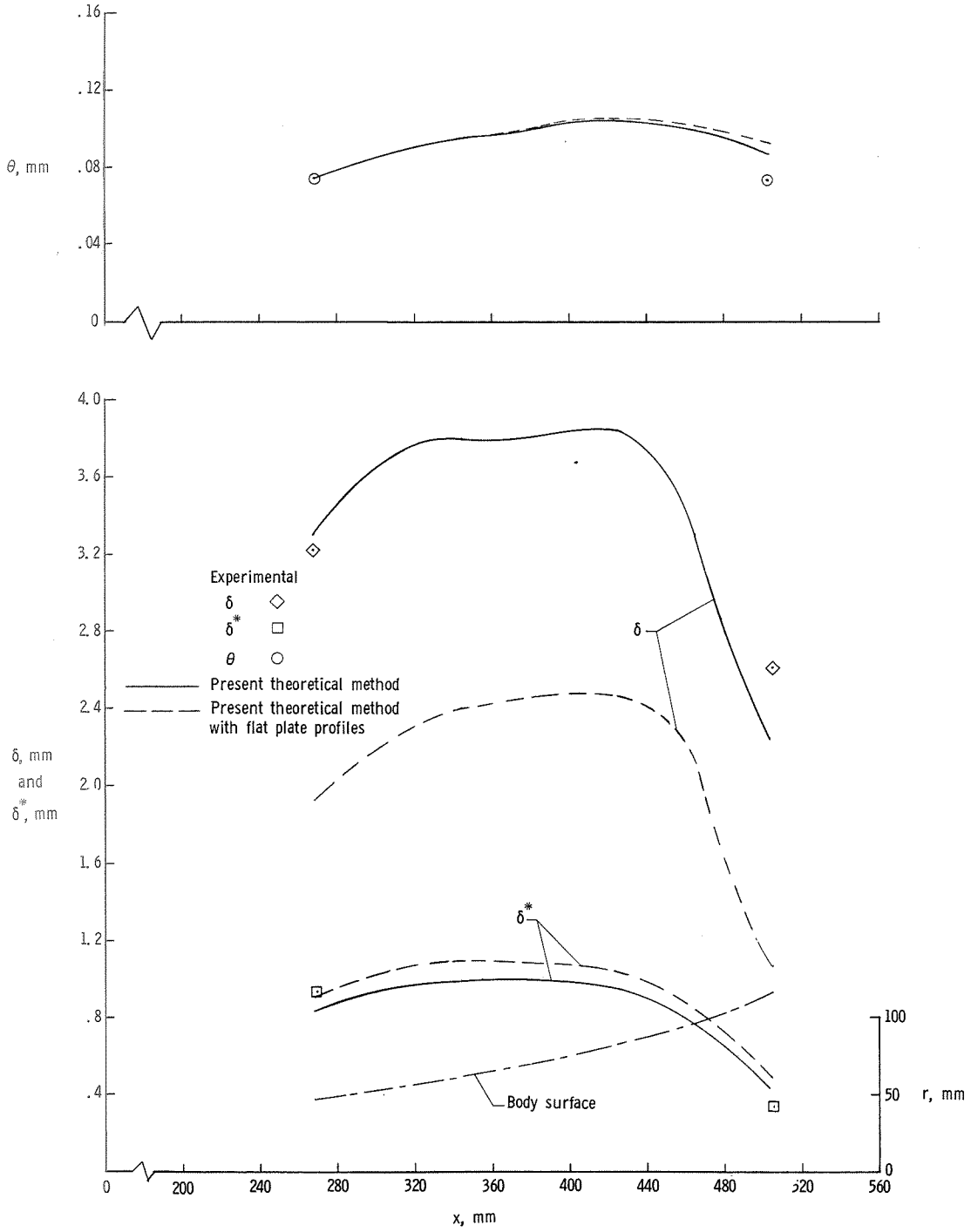

Figure 9.- Boundary-layer development on axisymmetric body of reference 25. $M_\delta = 5.98$; uncooled.

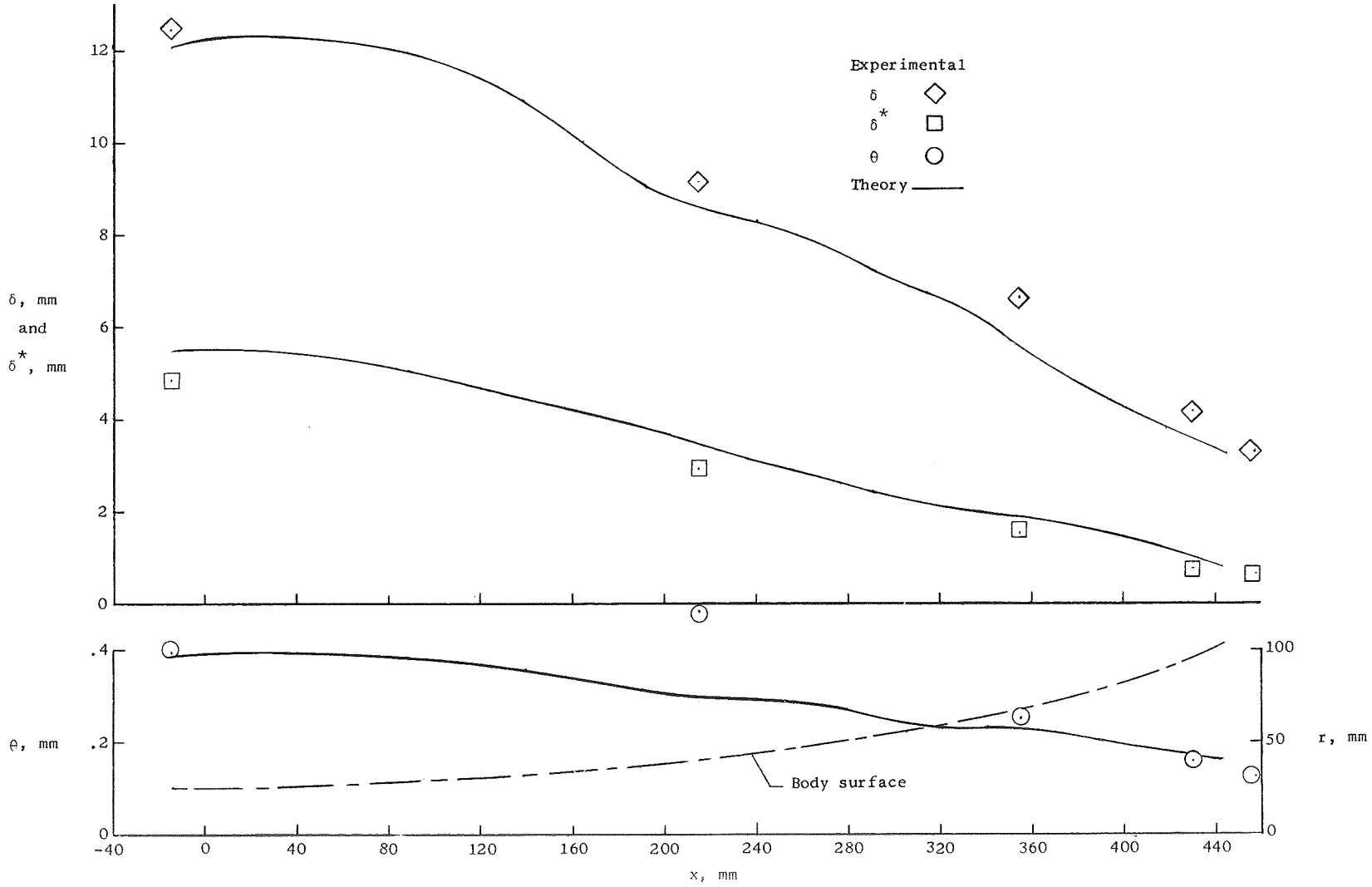

(a) $M_\delta = 5$; uncooled.

Figure 10.- Boundary-layer development on axisymmetric bodies of reference 26.

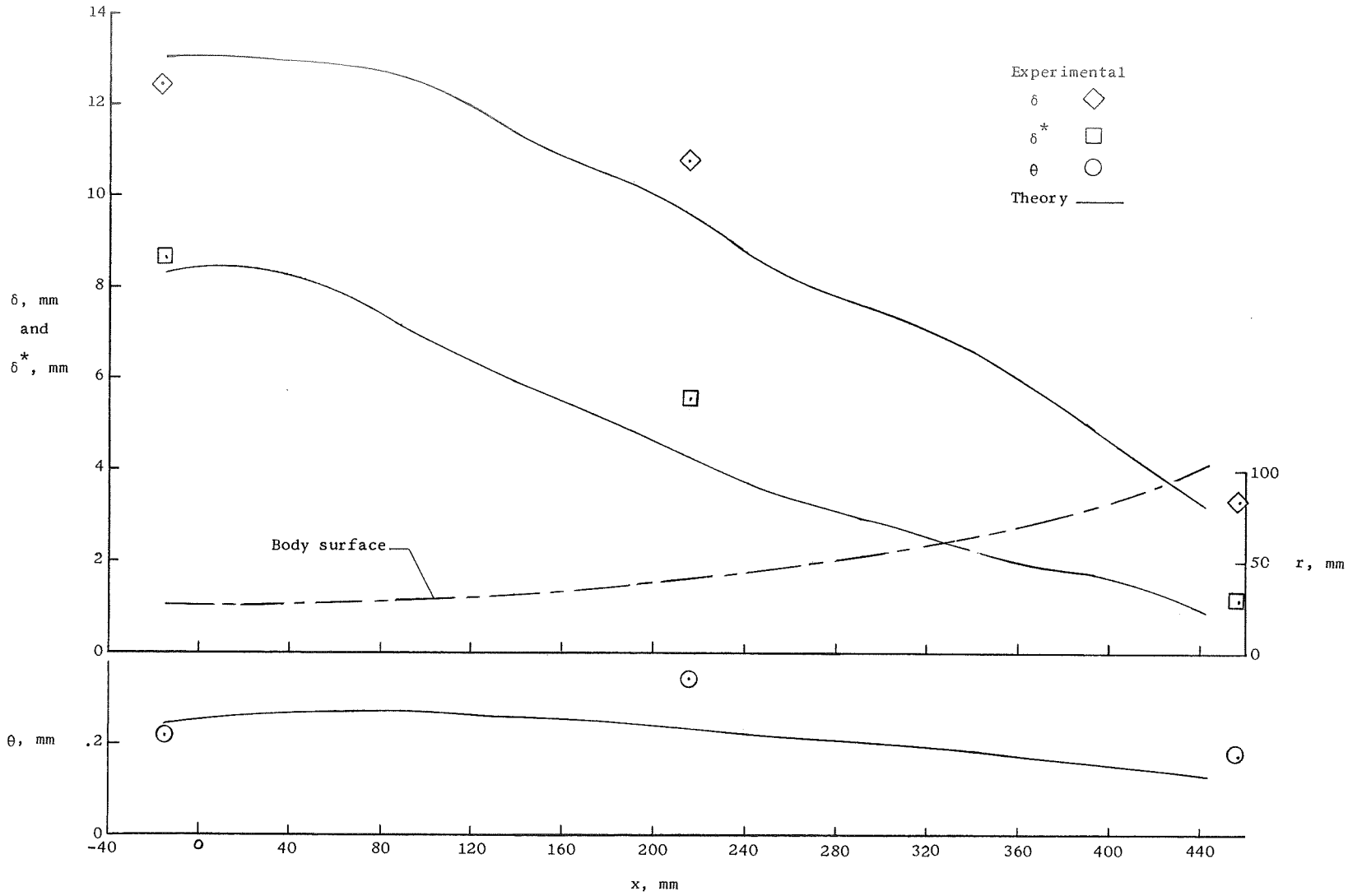

(b) $M_\delta = 6$; uncooled.

Figure 10.- Continued.

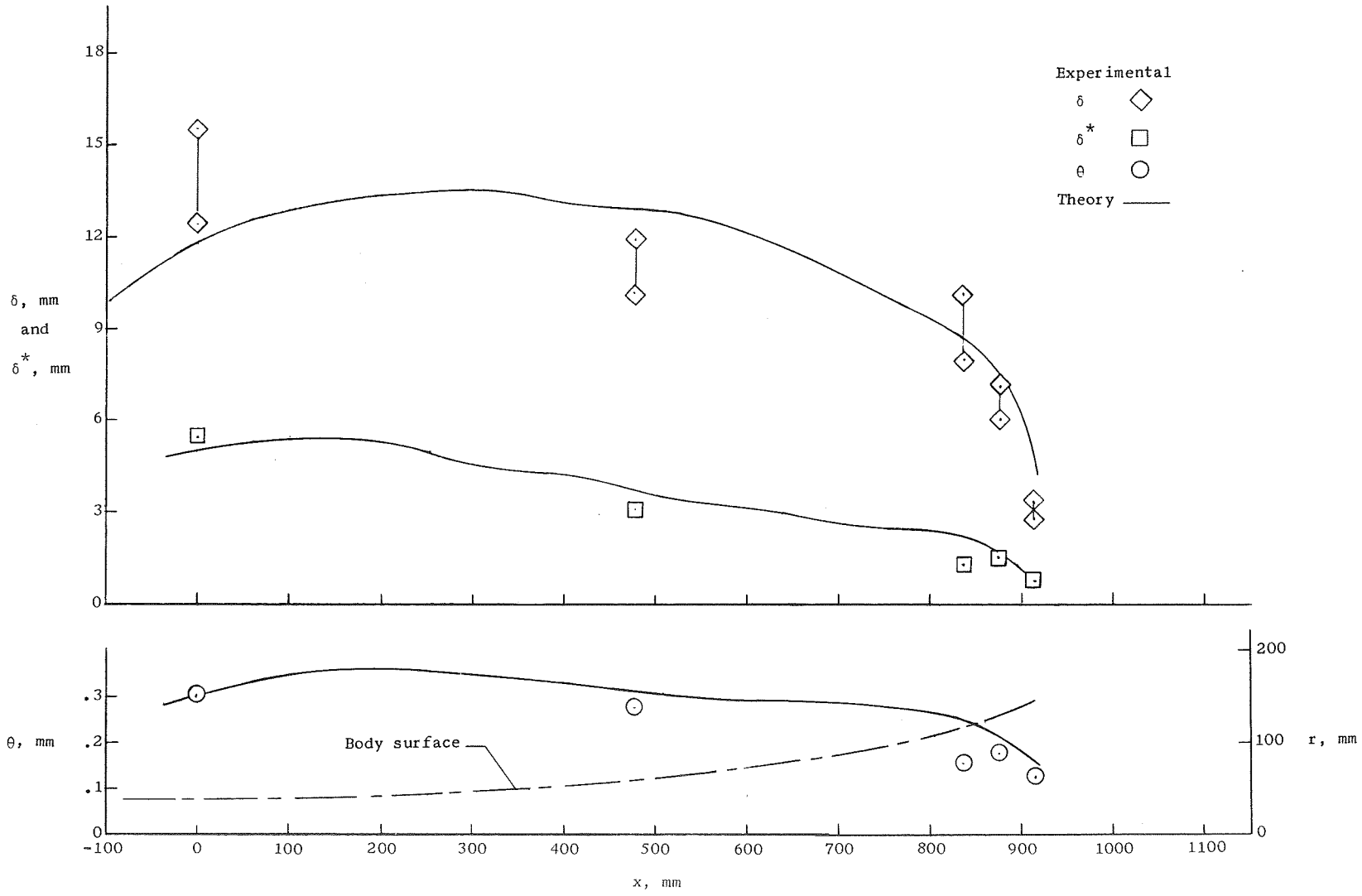

(c) $M_\delta = 6$; cooled.

Figure 10.- Continued.

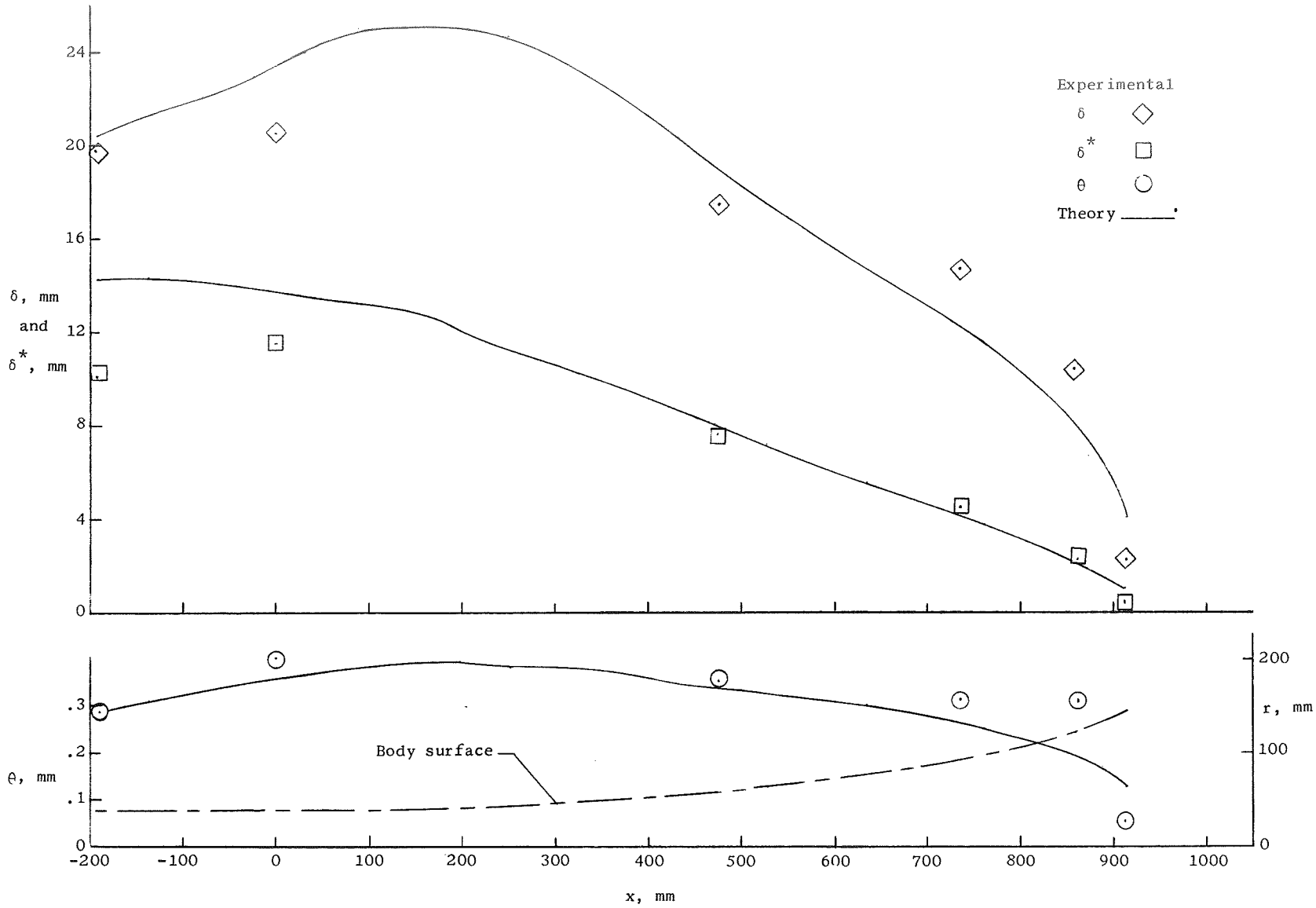

(d) $M_\delta = 8$; cooled.

Figure 10.- Concluded.

NATIONAL AERONAUTICS AND SPACE ADMINISTRATION
WASHINGTON, D. C. 20546

OFFICIAL BUSINESS
PENALTY FOR PRIVATE USE $300

FIRST CLASS MAIL

POSTAGE AND FEES PAID
NATIONAL AERONAUTICS AND
SPACE ADMINISTRATION

POSTMASTER: If Undeliverable (Section 158 Postal Manual) Do Not Return

"The aeronautical and space activities of the United States shall be conducted so as to contribute . . . to the expansion of human knowledge of phenomena in the atmosphere and space. The Administration shall provide for the widest practicable and appropriate dissemination of information concerning its activities and the results thereof."

—NATIONAL AERONAUTICS AND SPACE ACT OF 1958

NASA SCIENTIFIC AND TECHNICAL PUBLICATIONS

TECHNICAL REPORTS: Scientific and technical information considered important, complete, and a lasting contribution to existing knowledge.

TECHNICAL NOTES: Information less broad in scope but nevertheless of importance as a contribution to existing knowledge.

TECHNICAL MEMORANDUMS: Information receiving limited distribution because of preliminary data, security classification, or other reasons.

CONTRACTOR REPORTS: Scientific and technical information generated under a NASA contract or grant and considered an important contribution to existing knowledge.

TECHNICAL TRANSLATIONS: Information published in a foreign language considered to merit NASA distribution in English.

SPECIAL PUBLICATIONS: Information derived from or of value to NASA activities. Publications include conference proceedings, monographs, data compilations, handbooks, sourcebooks, and special bibliographies.

TECHNOLOGY UTILIZATION PUBLICATIONS: Information on technology used by NASA that may be of particular interest in commercial and other non-aerospace applications. Publications include Tech Briefs, Technology Utilization Reports and Technology Surveys.

Details on the availability of these publications may be obtained from:

SCIENTIFIC AND TECHNICAL INFORMATION OFFICE

NATIONAL AERONAUTICS AND SPACE ADMINISTRATION

Washington, D.C. 20546